LOW-FREQUENCY NOISE CHARACTERISATION AND MODELLING OF METAL-OXIDE-SEMICONDUCTOR FIELD-EFFECT TRANSISTORS

by

Jason Thomas Hodges

Dissertation submitted in fulfilment of the requirements

for the degree of

MASTER OF RESEARCH

School of Engineering
Faculty of Science and Engineering
Macquarie University
Sydney, Australia

September 2017

ACKNOWLEDGMENTS

I am very fortunate to have received continuous guidance and support from many people to whom I admire throughout this work. First, I would like to show gratitude toward my head supervisor, Prof. Michael Heimlich. Without his tireless efforts this work would simply not exist.

I am most appreciative of having Dr. Sourabh Khandelwal come on-board as lead supervisor in the early beginnings of this work. To whom I will always remain indebted to for his patience and thought-provoking discussions throughout the course of this work. I have the utmost respect for his genuine interest in this work and I can not thank him enough.

I would like to thank Brendan Whelan, Shaozhong Li, and Don Swanner of Analog Devices, Inc., (formerly Linear Technology Corporation) who, in conjunction with Prof. M. Heimlich, are responsible for the existence of this work. Furthermore, I am grateful for their gratuitous support throughout the entirety of this work.

I had the pleasure of working with Prof. Jonathan B. Scott from the University of Waikato in Hamilton, New Zealand during the early stages of this work. His genuine enthusiasm and interest toward all things electronic was a refreshing reminder as to why I initially chose to enter the field of electronic engineering.

I would also like to thank Dr. Oya Sevimli of MACOM Technology Solutions to whom I would not be where I am today without her endless support.

Last but not to say the least, my family. Wayne, Kim, Matthew, Nicole, Mitch, and Zahlia. To all of whom I say thank you for your endless love and support at every step of the way throughout my time at Macquarie University.

STATEMENT OF CANDIDATE

I, Jason Thomas Hodges, declare that this thesis entitled "**Low-Frequency Noise Characterisation and Modelling of Metal-Oxide-Semiconductor Field-Effect Transistors**" has not previously been submitted for a degree nor has it been submitted as part of the requirements for a degree to any other university or institution other than Macquarie University.

In addition, I certify that all information sources and literature used are indicated in the thesis.

Jason Thomas Hodges

September 25, 2017

ABSTRACT

The work presented here develops a systematic and self-consistent framework for the characterisation and modelling of low-frequency noise that is present in Silicon Metal-Oxide-Semiconductor Field-Effect Transistors (Si MOSFETs). The techniques and procedures developed in this work are general and can typically be applied to the low-frequency noise characterisation of any semiconductor device.

In general, there are three topics presented in this work. First, a mathematical review of the mechanisms involved with the analysis of noise is presented. Furthermore, various types of intrinsic noise sources are mathematically reviewed.

Second, an insight into the hardware associated with the characterisation of low-frequency noise is given. Techniques and methods for validating the noise floor of a low-frequency noise measurement system are presented.

Third, a systematic approach for validating the measured noise data is presented by means of manually modelling the measured data. This is opposed to the use of software packages where automatic parameter extraction is typically performed.

This work, in its entirety, is shown to hold for a given Si n-channel MOSFET device.

Contents

List of Figures

Chapter 1

Introduction

1.1 Aim

The phenomenon of noise is a fundamental problem in science and engineering, recognised and underlined in a variety of fields such as nanoelectronics, biological systems, and telecommunications. The perturbations that may be present in an electronic system which originate from external sources are not considered as noise in this work. Intrinsic noise in an electronic device is a random, spontaneous fluctuation of a deterministic signal inherent to the physics of the device. Intrinsic noise cannot be eliminated, however it is possible to reduce it with improvements in device technologies. Therefore, it is noise which ultimately limits the accuracy of any measurement and sets the lower limits to the strength of signals that can be detected and processed in an electronic system. The low-frequency noise originating from within semiconductor devices is currently a severe obstacle in radio frequency (RF)/wireless circuits. In 2005, Deen and Marinov [1] made the prediction that low-frequency noise will be of great concern to digital electronics due to the downscaling of the physical device dimensions which entails a downscaling of the voltages at which the advanced technology is designed to operate at. In turn, this leads to lower signal-to-noise ratios.

Figure 1.1 illustrates such concerns of device reliability, indicating that the relative noise level is already a problem in analog and RF applications with a trend showing that the limit of reliable device operation in digital applications has already been exceeded.

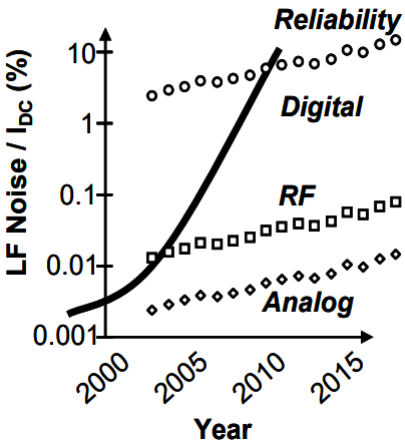

Figure 1.1: Lattice plot, showing the relative low-frequency noise magnitude and the reliability limits for various applications [1].

It is this trend that stimulates the need for improvements in the characterisation and modelling of low-frequency noise. This work aims to provide a systematic approach for such needs in the characterisation and modelling of $1/f$ (flicker) noise.

1.2 Thesis organisation

This thesis includes five (5) chapters and three (3) appendices. The appendices are referred to as required throughout the thesis with the exception of Appendix C, which is the list of abbreviations.

Chapter 1 introduces the thesis as a whole. In **Chapter 2**, the mathematical tools which are required for the analysis of noise are reviewed. An interpretation of the derivation of thermal noise pertaining to the methodology given in [2] is presented. **Chapter 3** presents the hardware which is typically associated with low-frequency noise measurements. Furthermore, techniques and methods for validating the hardware are given.

Chapter 4 presents a self-consistent framework for the verification of measured data, which makes use of [3]. **Chapter 5** draws a conclusion and presents topics of interest for future work.

Chapter 2

Noise mechanisms

Voltages and currents generated in an electronic device or circuit show perturbations around their nominal DC values due to fluctuations in the physical processes governing the transportation of electrical energy. While noise is typically seen as an unwanted phenomenon, it is plausible to use a noise signal for system evaluation and in turn gain insight into the system properties [4]. Characterisation of low-frequency noise in electronic devices provides crucial information of device physics and reliability such as scattering processes, traps and defects [5].

2.1 A mathematical review of noise

A key tool in the analysis of noise is the exploitation of the fact that noise, in general, is a stationary random process. However, if the process under examination is that of a non-stationary process, it is vital that the analysis is done in 'windows' of time where the process appears as stationary. This allows for simplification in the analysis process.

Consider a periodic signal, $X(t)$, as seen in Figure 2.1.

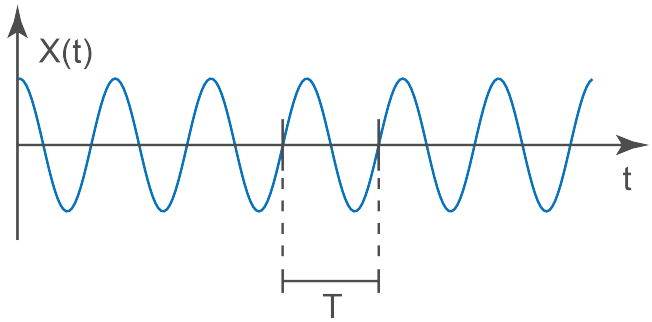

Figure 2.1: Periodic signal with a period of T.

The average power of $X(t)$ is given by

$$P_{av} = \frac{1}{T}\int_{-T/2}^{T/2} X^2(t)dt = \overline{X^2} \tag{2.1}$$

However a random process, such as the voltage across a resistor, at first glance is not a periodic signal as illustrated in Figure 2.2. Thus,

$$\overline{X^2} = \lim_{T\to\infty}\frac{1}{T}\int_{-T/2}^{T/2} X^2(t)dt \tag{2.2}$$

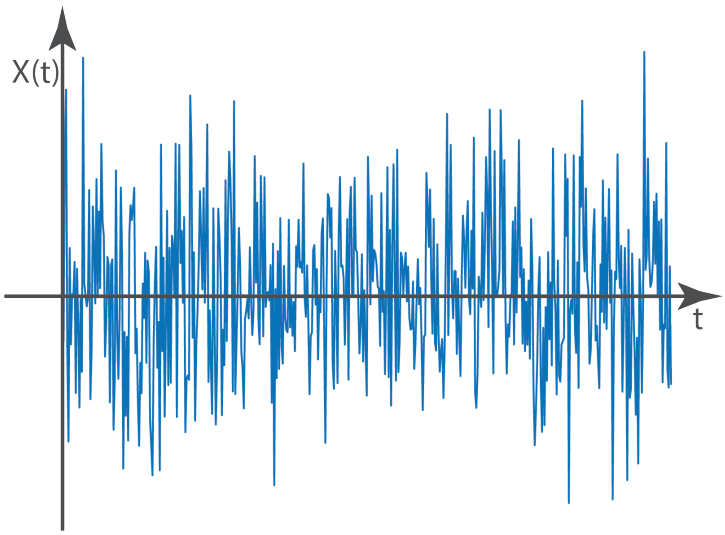

Figure 2.2: Example random process, $X(t)$.

Equation (2.2) implies that a random process is indeed a periodic signal with a period that is infinitely long.

While Equations (2.1) and (2.2) are valid, they do not provide any information in regards to the frequency content of the signal under analysis. Thus, the need for a more generalised concept.

2.1.1 Power Spectral Density (PSD)

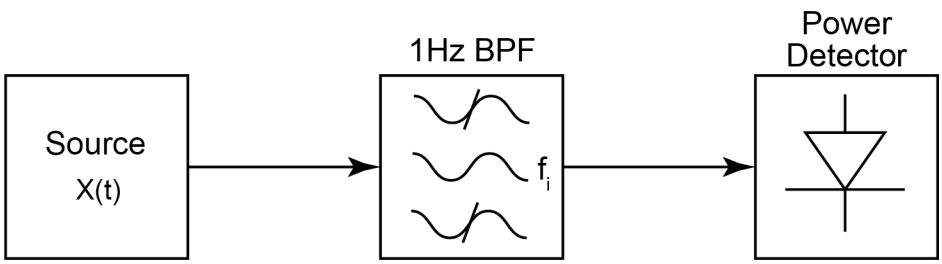

Figure 2.3: Block diagram which yields PSD.

Consider the signal, $X(t)$ from Figure 2.2. $X(t)$ is fed into a band-pass filter (BPF) which has a bandwidth of 1Hz. The pass-band frequency of the 1Hz BPF, f_i, is shifted up and down in order to obtain the given power at each frequency. The output of the BPF is then fed into a power detector and the output of the power detector is plotted, the result would be as seen in Figure 2.4.

It was seen that Equation (2.2) can give the average power of the signal, however, it can only do as such for any given period of time. The autocorrelation function, see Equation (2.3), expands on this notion by analysing how the signal is changing over time.

Consider the modified form of Equation (2.2).

$$\overline{X^2} = \lim_{T\to\infty} \frac{1}{T} \int_{-T/2}^{T/2} X(t)X(t+\tau)dt = R_{xx}(\tau) \tag{2.3}$$

Equation (2.3) is known as the autocorrelation function.

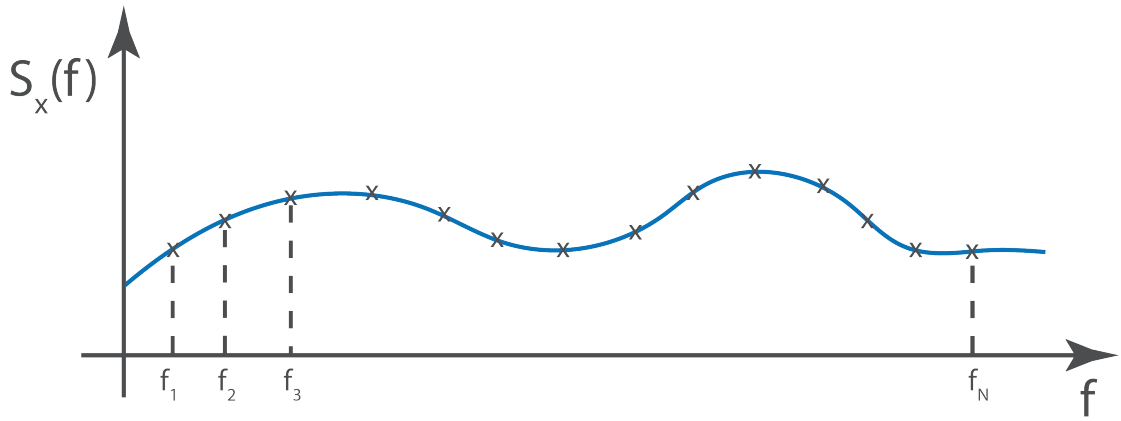

Figure 2.4: Response from the output of the power detector in 2.3.

Figures 2.3 and 2.4 illustrate the fundamental definition of the power spectral density. It can be mathematically proven that the PSD is directly related to the autocorrelation function. This is known as the Wiener-Khinchin theorem.

$$S_x(f) = \mathscr{F}\left\{R_{xx}(\tau)\right\} = \int_{-\infty}^{\infty} R_{xx}(t)e^{-j2\pi tf}dt, \tag{2.4}$$

which states that the PSD of a signal is a Fourier transform of the autocorrelation function.

2.2 Fundamental noise sources

2.2.1 Thermal noise

Consider a standard resistor that would be used in an electronic circuit. Typically these can be composed of some resistive material such as carbon. If a voltage source is placed across the resistor, then exhibited within this resistive material is a cluster of charged particles known as free electrons. Unless the resistor is stored at absolute zero, these electrons move around. The motion of these charged particles, in particular the variation that occurs, creates fluctuations in the density of the electrons which in turn creates

fluctuations in the voltage across the resistor. This notion was first discovered by Walter Schottky in 1918 [6]. However it was the work of John B. Johnson and Harry Nyquist who established this concept in 1928 [7, 8].

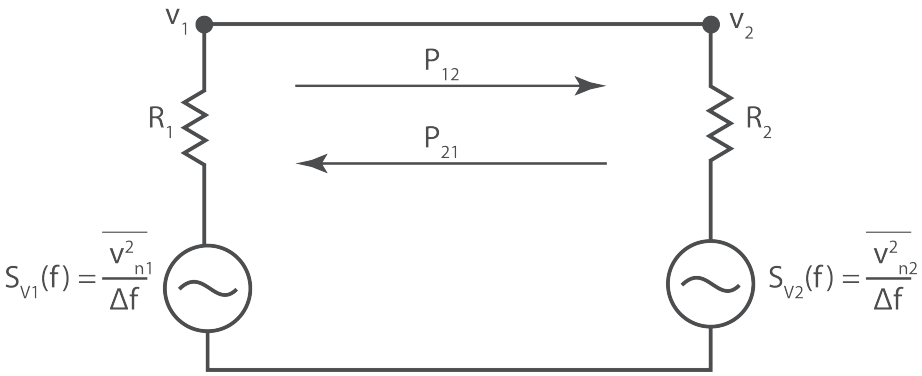

Figure 2.5: Two resistors, R_1 and R_2 and their associated noise sources connected.

Figure 2.5 illustrates two resistors at the same temperature, T, connected to each other. Also included are the noise sources that are associated with each resistor due to the thermal movement of the free electrons. The power generated from the noise source of R_1 corresponds to P_{12}, similarly P_{21} corresponds to R_2.

Hence,

$$P_{12} = \frac{\overline{v_2^2}}{R_2} = \frac{\overline{v_1^2}}{R_2} \cdot \frac{R_2^2}{(R_1+R_2)^2} = \overline{v_1^2} \cdot \frac{R_2}{(R_1+R_2)^2}$$

Similarly,

$$P_{21} = \overline{v_2^2} \cdot \frac{R_1}{(R_1+R_2)^2}$$

Thus, $P_{12} = P_{21}$. It is forbidden by the second law of thermodynamics [9] that there can exist some instance for which $P_{12} \neq P_{21}$. This implies that,

$$\overline{v_n^2} \propto R \tag{2.5}$$

Therefore it can be seen from Equation (2.5) that the voltage noise of a resistor is proportional to the value of resistance.

Consider,

$$(P_{12} - P_{21}) \propto (T_1 - T_2), \tag{2.6}$$

where T_1 and T_2 correspond to the absolute temperature of R_1 and R_2, respectively. Equation (2.6) is derived from the Planck distribution where it is stated that the mean thermal energy contained in each electromagnetic mode is [10]

$$\langle E(f) \rangle = \frac{hf}{e^{hf/k_B T - 1}} \approx k_B T \tag{2.7}$$

Hence by letting $T_2 = 0$ K, Equation (2.6) reduces to,

$$\begin{aligned} P_{12} &\propto T_1 \\ \Rightarrow \overline{v_n^2} &\propto T \end{aligned} \tag{2.8}$$

Thus it can be concluded that the thermal noise which is generated by a resistor is dependent on resistance and temperature, RT.

$$\overline{v_n^2} \propto RT \tag{2.9}$$

Consider the circuit given in Figure 2.6.

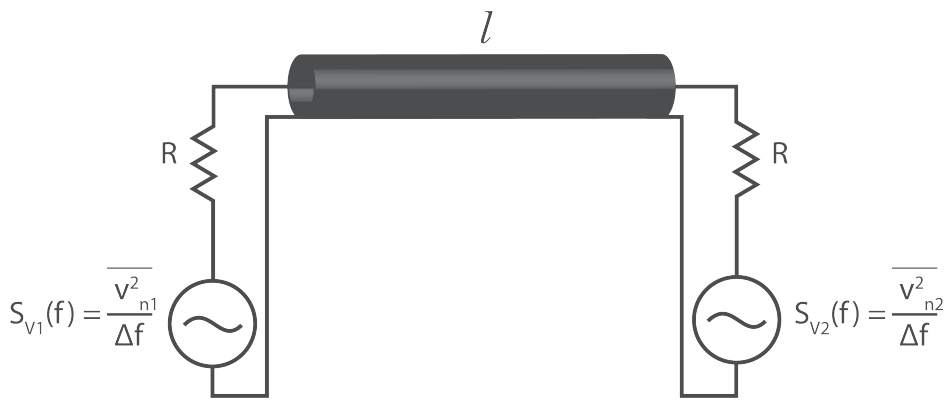

Figure 2.6: Transmission line of length l terminated on each side by a resistance R.

Let the resistance R be perfectly matched to the transmission line such that there are no reflections. Which gives

$$R = \sqrt{\frac{L}{C}} \tag{2.10}$$

Hence,

$$P_{12} = \frac{\overline{v_{n1}^2}}{4R} \tag{2.11}$$

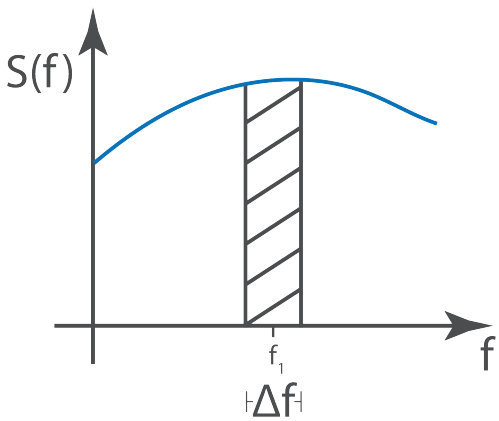

Figure 2.7: Example PSD of Figure 2.6 for an interval Δf.

The power transferred from $S_{v1}(f)$ to $S_{v2}(f)$ (left to right) in an infinitesimal interval, Δf as depicted in Figure 2.7, is given by

$$\Delta P = \frac{S_v(f)}{4R} \cdot \Delta f \tag{2.12}$$

Consider the amount of energy which is inside the transmission line at frequency f, given by

$$\Delta E = \frac{2l}{v} \cdot \Delta P, \tag{2.13}$$

where l is the length of the transmission line, v is the velocity of propagation, thus $\frac{l}{v}$ is the time in which it takes the energy to travel left to right through the transmission line. As there are two sources on each end of the transmission line, there is twice as much energy within the transmission line hence the need to multiply by a factor of two.

Equation (2.13) then becomes

$$\Delta E = \frac{2l}{v} \cdot \frac{S_v(f)}{4R} \Delta f \tag{2.14}$$

which is the total amount of energy within the transmission line.

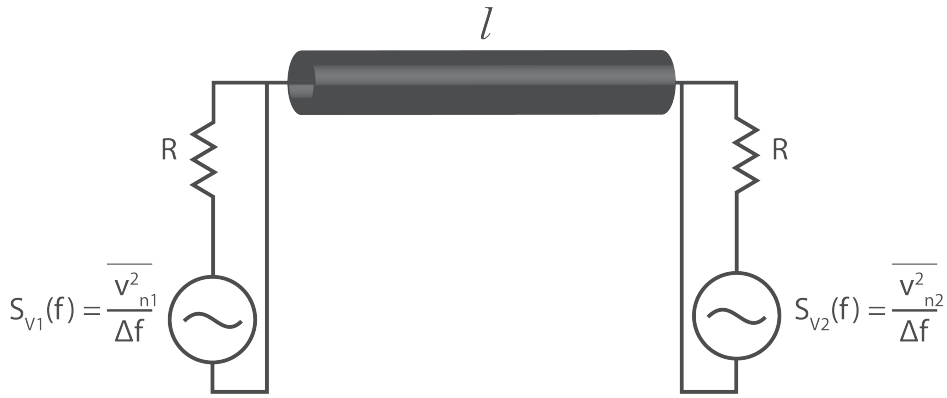

Figure 2.8: Transmission line of length l terminated on each side by a short to ground after some time period, t.

Consider the circuit of Figure 2.8. If a switch were to be placed at both ends of the transmission line and at some point in time both switches were to be closed causing a short circuit to ground then the energy within the transmission line would become trapped, thus creating standing-wave patterns as depicted in Figure 2.9.

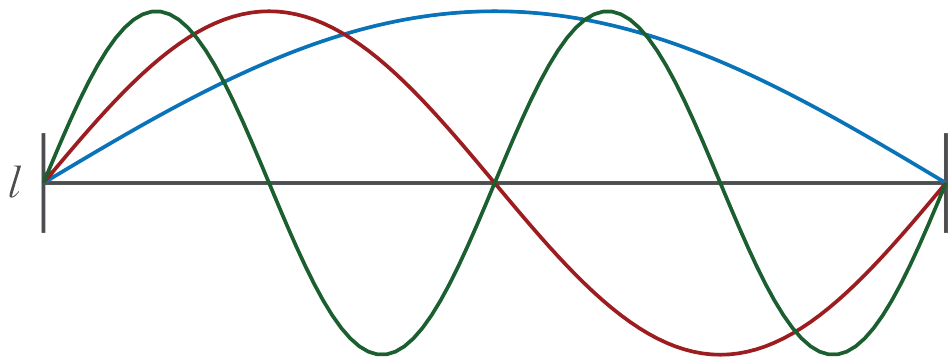

Figure 2.9: Example of fundamental, second and third modes in a given length, l, of a transmission line.

where,

$$l = \frac{n\lambda}{2} \qquad ; n \in \mathbb{N} \tag{2.15}$$

The frequencies of these modes are given by

$$f = n\frac{v}{2l} \tag{2.16}$$

In order to determine the quantity of modes, m, within a given infinitesimal interval, Δf, the following is used

$$m = \frac{\Delta f}{v/2l} = \frac{2l}{v}\Delta f \tag{2.17}$$

As there exists both magnetic energy storage and electrical energy storage within the transmission line, the quantity of modes is therefore doubled. This pertains to

$$\Delta E = 2m \cdot \frac{KT}{2} = \frac{2l}{v}KT\Delta f \tag{2.18}$$

where ΔE is the amount of energy within the infinitesimal interval Δf. By equating Equation (2.14) and (2.18), the following can be obtained.

$$\begin{aligned} \Delta E &= \frac{2l}{v} \cdot \frac{S_v(f)}{4R}\Delta f = \frac{2l}{v}KT\Delta f \\ \Rightarrow S_v(f) &= \boxed{4KTR} \\ \Rightarrow S_i(f) &= \boxed{\frac{4KT}{R}} \end{aligned} \tag{2.19}$$

Thus, arriving at the definition for the PSD of thermal noise, where K is Boltzmann's constant (1.38 x 10^{-23} J/K), T is the absolute temperature and R is resistance. $S_v(f)$ and $S_i(f)$ are in units of V^2/Hz and A^2/Hz, respectively.

2.2.2 Shot noise

Shot noise is typically associated with devices containing a *p-n* junction. This is based on the fact that the current which flows across a *p-n* junction is not continuous due to the discrete nature of electrons. Rather, the current across a *p-n* junction is given by the number of carriers, each carrying the charge q, flowing through the junction independently

and at random. A shot noise current is generated when the electrons cross the p-n junction. The PSD of shot noise current is obtained by [2]

$$S_i(f) = 2qI \tag{2.20}$$

where q ($q = 1.6 \times 10^{-19}C$) is the electron charge and I is the current in DC operating conditions or the instantaneous current in dynamic operating conditions [11].

A p-n junction behaves like a non-linear resistor. Such that the physics of shot noise are closely related to that of the thermal noise phenomenon. Current can flow through a resistor in two directions, while a p-n junction only allows current to flow in one direction (disregarding reverse leakage current) thus the PSD of shot noise is half that of thermal noise.

2.2.3 Generation-recombination noise

Generation-recombination (g-r) noise originates from electron trap sites which randomly capture and emit charge carriers (free electrons). This causes a fluctuation in the number of charge carriers available for current transport. These traps exist due to defects in the manufacturing process. Such defects may include heavy ion implantation, or unintentional side-effects such as surface contamination. As the effects are due to errors in the manufacturing process, offending devices can be detected and removed during manufacturing. The PSD of g-r noise is given by [2]

$$S_N(f) = \overline{4\Delta N^2} \cdot \frac{\tau_i}{1 + \omega^2 \tau_i^2}, \tag{2.21}$$

where τ_i is the time constant associated with the ith trap. G-r noise posses a Lorentzian shaped PSD as seen in Figure 2.10

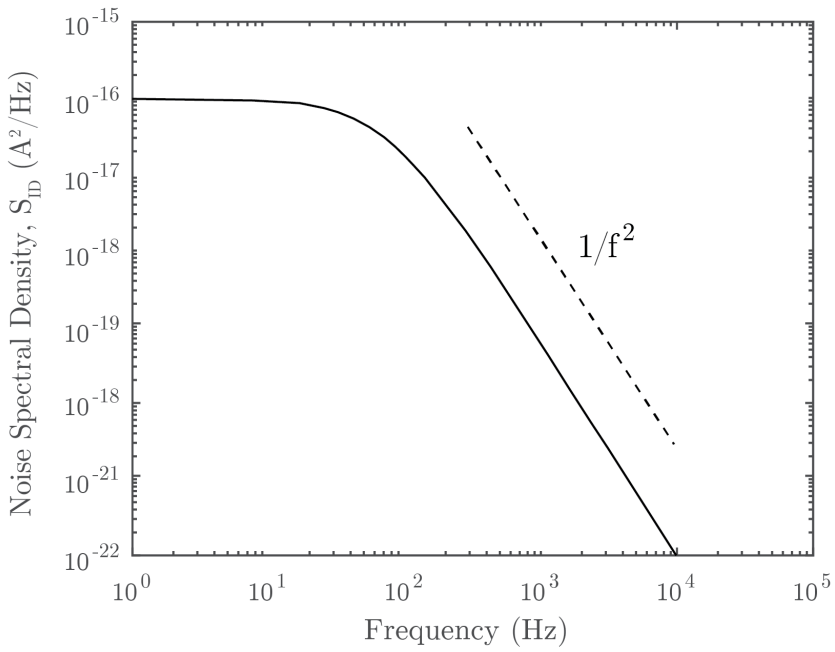

Figure 2.10: Lorentzian shaped PSD of g-r noise.

2.2.4 $1/f$ noise

$1/f$ noise, also known as flicker noise, was discovered by John B. Johnson in 1925 [12] and interpreted by William Schottky in 1926 [13]. The physical mechanisms of $1/f$ noise in semiconductors have been the subject of intensive study for several decades now. There are several theories, some with conflicting conclusions and several remaining unresolved issues. The principal characteristic of $1/f$ noise is that it has a $1/f^{\alpha}$ PSD with α close to 1, typically in the range of 0.7-1.3. The PSD of $1/f$ noise, in its general form, is given by [14]

$$S_i(f) = \frac{KI^{\beta}}{f^{\alpha}}, \tag{2.22}$$

where K is a constant and β is a current exponent.

The current density in an n-type semiconductor is given by the following [5]

$$J = \sigma E = (qn\mu_n + qp\mu_p)E \approx nq\mu_n E, \tag{2.23}$$

where σ is the conductivity of the conductor, E is the electric field intensity voltage/length, q is the absolute charge of each electron and hole, n and p are the concentration of mobile electrons and holes respectively, and μ_n and μ_p are the mobility of electrons and holes respectively.

By analysing Equation (2.23), it can be seen that there are essentially two physical mechanisms that could correspond to any fluctuations in the current: fluctuations in the number of charge carriers (g-r noise) [15, 16] or fluctuations in the mobility of the charge carriers [17, 18]. The PSD of g-r noise was given in Equation (2.21). By expanding on this for an infinite amount of traps gives the following

$$S_{Total}(f) = \int_0^\infty \frac{B}{\tau_i} \cdot \overline{4\Delta N^2} \cdot \frac{\tau_i}{1+\omega^2\tau_i^2} \; d\tau_i \tag{2.24}$$

where $\frac{B}{\tau_i}$ is some constant which corresponds to the total amount of traps with a time constant τ_i that occur. $S_{Total}(f)$ coincides to the number fluctuation theory.

An example is given in Figure 2.11 where the g-r noise from five individual traps with different time constants ($\tau_1 - \tau_5$) sum up to a $1/f^\alpha$ PSD with α close to 1.

The second mechanism, mobility fluctuation, was first described by Hooge in 1969 [20] with the empirical formula for a MOSFET

$$\frac{S_{I_D}}{I_D^2} = \frac{q\alpha_H}{fWLQ_i}, \tag{2.25}$$

where W and L are the physical width and length of the conduction channel, respectively. α_H is referred to as the Hooge parameter. Hooge first proposed that this parameter were constant and equal to 2×10^{-3} [17]. However, it was later found that α_H depends on the crystal lattice quality; values of several orders of magnitude lower have been reported in perfect materials [21]. Typical values for α_H range between 10^{-3} and 10^{-6} [22]. While $Q_i = C_{ox}(V_{GS} - V_{TH})$ for a MOSFET operating in the linear region, hence the normalised drain current noise is inversely proportional to the gate voltage overdrive (V_{OV}).

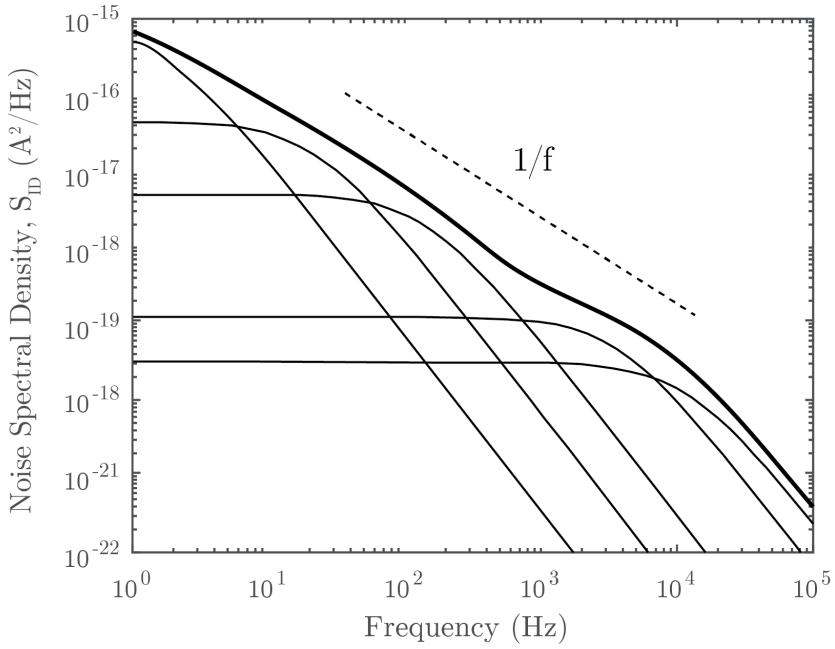

Figure 2.11: Superposition of five Lorentzian spectra which gives a total PSD showing an approximate $1/f$ dependence over several decades of frequency.

While there exists a unified flicker noise model [23], which has become widely accepted, there is yet to remain a universally accepted flicker noise model. The model of [23] incorporates both the mobility and number fluctuation mechanisms where it has been shown to hold for various MOSFET technologies [24].

2.3 Noise sources in MOSFETs

Figure 2.12 depicts an equivalent circuit of a MOSFET noise model. The series resistors R_D and R_S pertain to the thermal noise formula given in Equation (2.19) such that

$$S_{Ri}(f) = \frac{4KT}{R_i}, \tag{2.26}$$

where R_i is either R_D or R_S. However, g_{DS} also contributes to the overall thermal noise of the device.

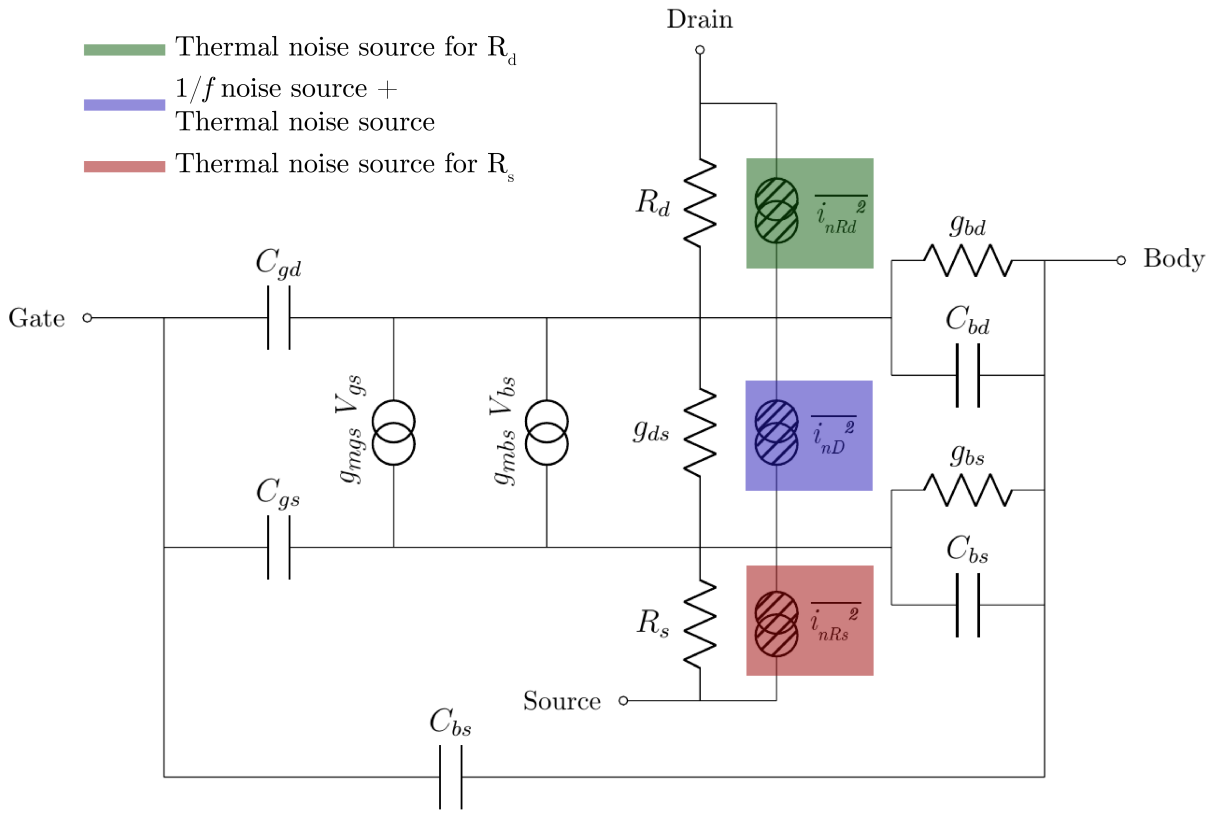

Figure 2.12: Equivalent circuit of a MOSFET noise model

The $1/f$ and thermal noise source (shown in blue in Figure 2.12) correspond to the drain current noise. The thermal noise source relates to the resistance of the conduction channel by the following

$$S_{channel} = \frac{8}{3} KT g_m, \tag{2.27}$$

where g_m is the transconductance of the MOSFET.

While the $1/f$ noise source is given by

$$S_{1/f} = \frac{KFI_D^{AF}}{f^{EF} C_{ox} L_{eff}^2} \tag{2.28}$$

Equation (2.28) is discussed in detail in chapter 4.

A MOSFET is a complex device comprised of a conduction channel which is controlled by the gate voltage (V_G). Typically the $1/f$ noise, which is seen at the drain terminal, is generated in the conduction channel. It is known that in low-frequency regimes, the $1/f$ noise dominates in MOSFETs. Evidently, this work is focused on the characterisation and modelling of $1/f$ noise, which is given in chapter 3 and 4.

Chapter 3

Noise characterisation

The measurement of noise is a complex task as the signals of interest are very weak, often as low as ~1 pA. Electrical equipment connected to mains power gives rise to disturbances at 50 Hz (60 Hz in some parts of the world), which often has harmonics at multiples thereof. The measurements are usually performed in the frequency domain by measuring the PSD with a dynamic signal analyser (DSA). However, the majority of DSA's that are available in industry make use of a cathode ray tube (CRT) for their display. CRT displays contain horizontal and vertical deflection circuitry which cause the electron beam to sweep across the display thus producing the image. Such circuitry produces electromagnetic interference (EMI); horizontal deflection is typically between 15 and 115 kHz (VLF) and vertical deflection between 50 and 92 Hz (ELF). Therefore, the measurement setup must be designed in such a way that external interferences do not affect the signals of interest. This can be done by either designing a low-pass filter which has a cut-off frequency of ~1 Hz or by biasing the device under test (DUT) from a battery operated power supply. This work makes use of a custom-made battery-operated power supply in order to bias the DUT, see Appendix B.1 for their schematics.

3.1 Measurement setup

The low-frequency noise measurement setup used in this work is depicted in Figure 3.1.

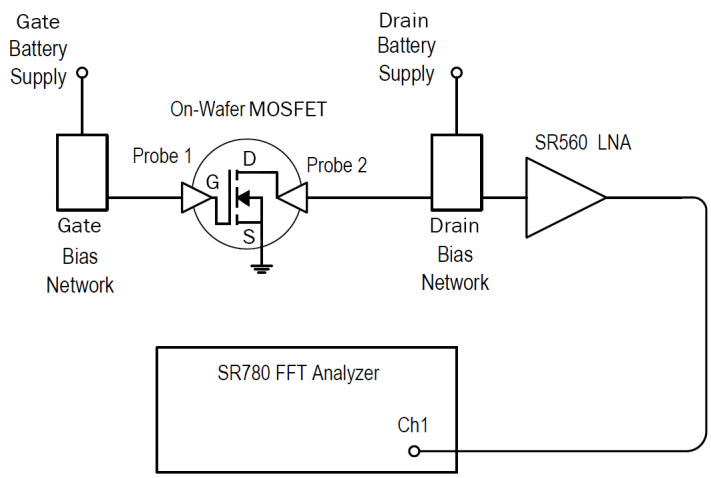

Figure 3.1: Low-frequency noise measurement setup.

The measurements were performed on-wafer by using a Cascade Microtech Summit 11000 series shielded probe station. Triax/BNC cables were used to connect the wafer probes to the custom-made battery-operated bias supplies. When adapting from triax to BNC it is essential that the correct type of adapter is used in order to prevent shorting the signal path to ground. As there are numerous types of triax to BNC adapters available, the correct and incorrect methods are illustrated in Figure 3.2.

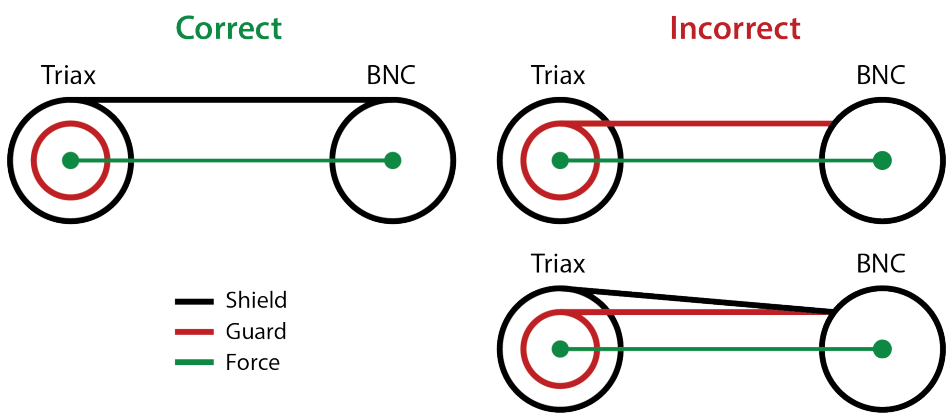

Figure 3.2: Correct and incorrect methods of adapting from triax to BNC.

The weak noise signal from the DUT is then amplified by a Stanford Research Systems low-noise voltage preamplifier, or simply, a LNA (SR560). The signal is then fed into a Stanford Research Systems DSA (SR780) which measures the PSD. The SR780 has a real-time bandwidth of DC – 102.4 kHz [25].

The LNA inevitably adds noise to the system. However, the SR560 contains its own internal battery supply and allows for the option of being battery powered in order to reduce its noise contribution to the measurement system. Furthermore, the internal noise of the amplifier sets the lower measurement limits (system noise floor) and therefore must be minimised. Figure 3.3 depicts the comparison of the noise contribution for different biasing options, with the LNA being operated via both mains and battery power.

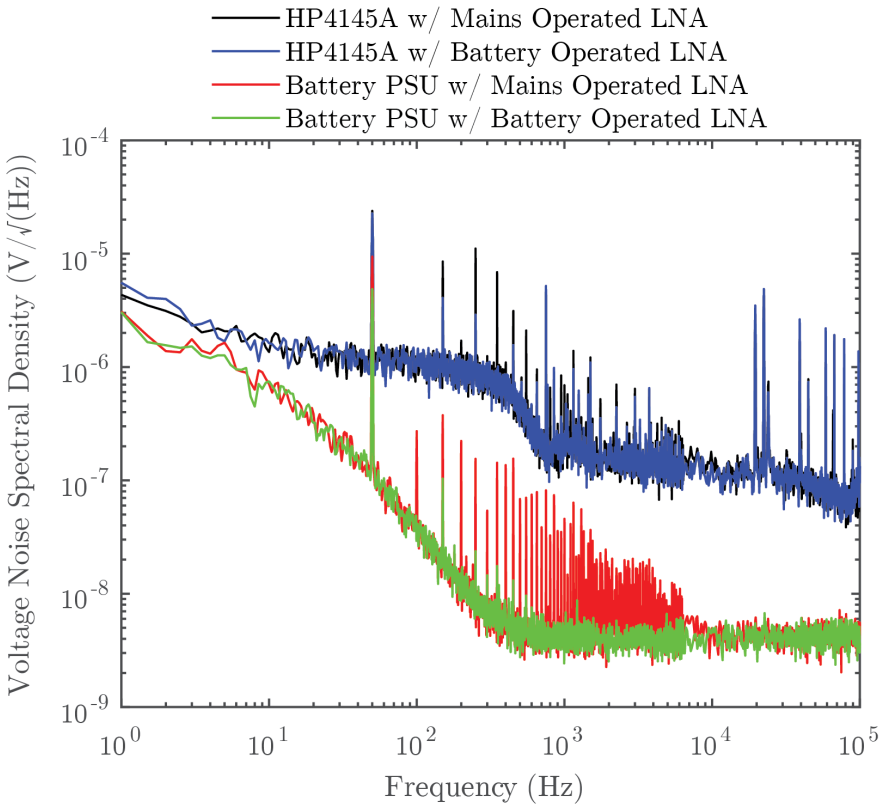

Figure 3.3: PSD comparison of HP4145A SMU and the custom-made battery-operated bias supply.

It can be seen that the noise floor of a HP4145A source measure unit (SMU) (black and blue traces) is ~2 orders of magnitude higher (at 1 kHz) than that of the custom-made battery-operated power supply unit (PSU). Thus it can be concluded that the custom-made battery-operated PSU in conjunction with the LNA also being powered by its own internal batteries contributes the least amount of noise to the measurement system, which offers a measured system noise floor of ~4 $\mathrm{nV}_{RMS}/\sqrt{Hz}$ at 1 kHz which corresponds with the documented noise floor of the LNA [26].

The measured data as seen by the DSA ($N_{measured}$) can be calculated by the following

$$N_{measured}(nV/\sqrt{Hz}) = \sqrt{4nV^2 + \left(\sqrt{4KTR_D}\right)^2 + (g_m R_D \cdot EINV)^2}, \tag{3.1}$$

where $4nV^2$ is the noise floor contribution of the LNA, g_m is the transconductance of the MOSFET under test, R_D is the load resistor (which is internal to the battery PSU), K is Boltzmann's constant, T is the absolute temperature and EINV is the equivalent input noise voltage of the MOSFET. Equation (3.1) pertains to the fundamental rule that noise adds in power.

Thus, the equivalent input noise voltage (EINV), or input referred voltage noise, of the measurement system of Figure 3.1 can be derived and is given by

$$EINV = \frac{2\sqrt{2^2 + 4KTR_D}}{g_m R_D} \tag{3.2}$$

Therefore, it can be concluded that it is desirable for the value of the load resistor, R_D, to be chosen such that it allows for maximum Υ, subject to varying g_m. Where Υ is equal to

$$\Upsilon = \frac{(g_m R_D EINV)^2}{4nV^2 + 4KTR_D} \tag{3.3}$$

It is important to note that the battery PSU has limited biasing capabilities. These limits pertain to a gate voltage (V_G) of 1 – 4 V and a drain voltage (V_D) of 1 – 5 V.

Figure 3.4 illustrates the absolute lower limits of EINV that the measurement system in Figure 3.1 is capable of performing corresponding to different values of R_D. It is important to note here that it is essential for R_D to be a wire-wound resistor as these posses the lowest noise index of available resistor compositions [27]. In the case of the measurement setup in Figure 3.1, R_D was chosen to be 680 Ω as this was the largest wire-wound resistor that was accessible.

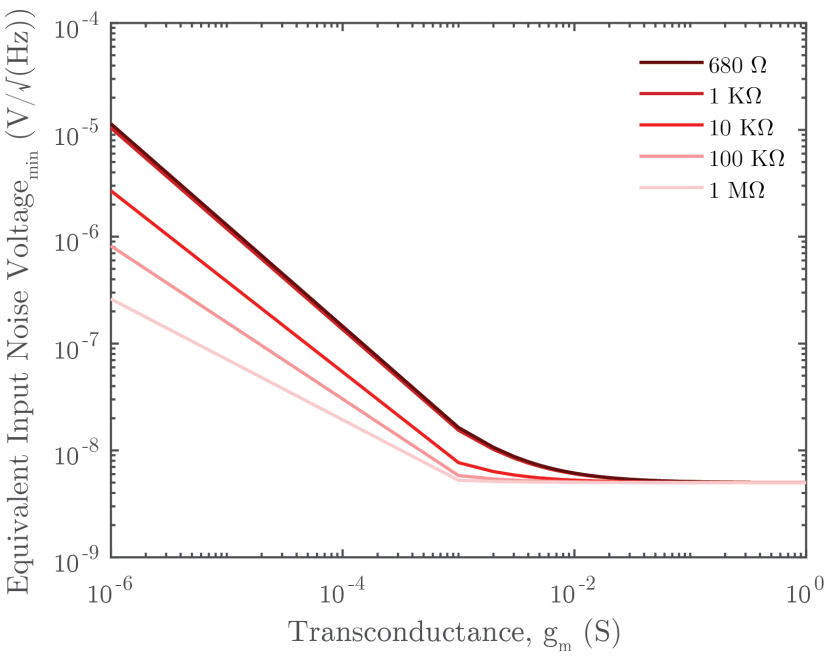

Figure 3.4: Minimum equivalent input noise voltage determined by load resistor.

3.2 Frequency domain analysis

Measurements performed in the frequency domain with the DSA are obtained by taking 50 averages of the input signal. This allows for more precise data to be gathered. The DSA is configured to apply a Hanning window to the signal. Walls *et al.* [28] investigated the effect of various types of windows on experimentally obtained data. The Hanning window gave the best results with the exception of the few lowest-frequency data points.

All measurements performed in this work were obtained using the Hanning window and the three lowest-frequency data points were omitted from the final dataset. The DSA displays the power spectral density in $V/\sqrt{Hz}$. Typical units for the power spectral density of a MOSFET are given in A^2/Hz (S_{ID}), thus some arithmetic is needed once the data has been gathered.

First, the gain of the LNA must be divided out in order to obtain the true PSD of the DUT. Typical gain settings of the LNA in this work are between 100 – 1000. The data is then squared, giving V^2/Hz (S_{VD}). Furthermore, the resistance of the DUT (R_{DS}) is obtained by the following

$$R_{DS} = 1/g_{DS}, \tag{3.4}$$

where g_{DS}, the output conductance, is given by

$$g_{DS} \triangleq \left.\frac{\partial I_D}{\partial V_{DS}}\right|_{V_{GS}} \tag{3.5}$$

Figure 3.5 depicts the measured versus the simulated output conductance of the DUT for the bias conditions of interest.

Thus, in order to ascertain the most accurate values of S_{ID}, the parallel combination of R_{DS} and R_D are used to obtain the total resistance at the load of the DUT, R_{load} given by

$$R_{load} = \frac{R_D \times R_{DS}}{R_D + R_{DS}} \tag{3.6}$$

Finally, S_{ID} can be obtained by the following

$$S_{ID} = \frac{S_{VD}}{R_{load}} \tag{3.7}$$

A typical drain current noise spectra is illustrated for an n-channel MOSFET (nMOS) device in Figure 3.6.

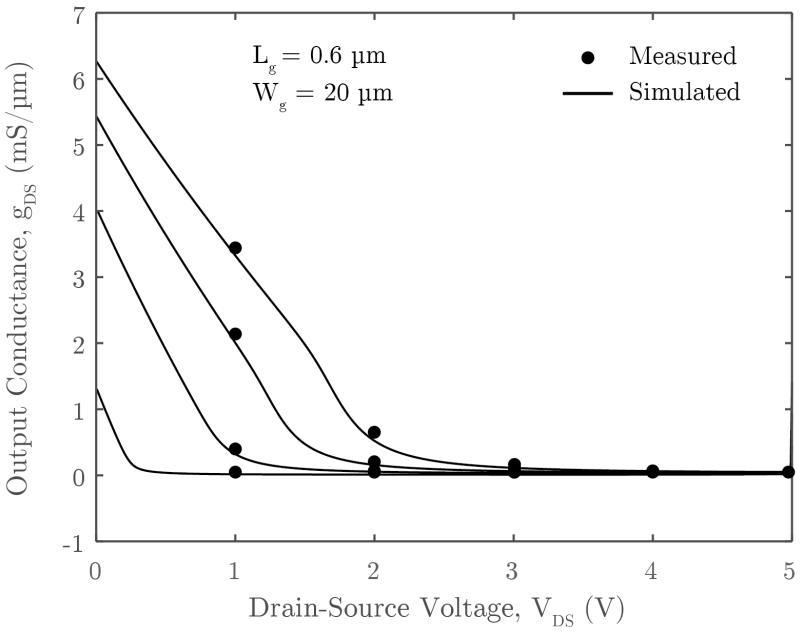

Figure 3.5: Measured vs simulated output conductance of industry supplied nMOS device, where L_g and W_g are the physical length and width of the gate channel, respectively.

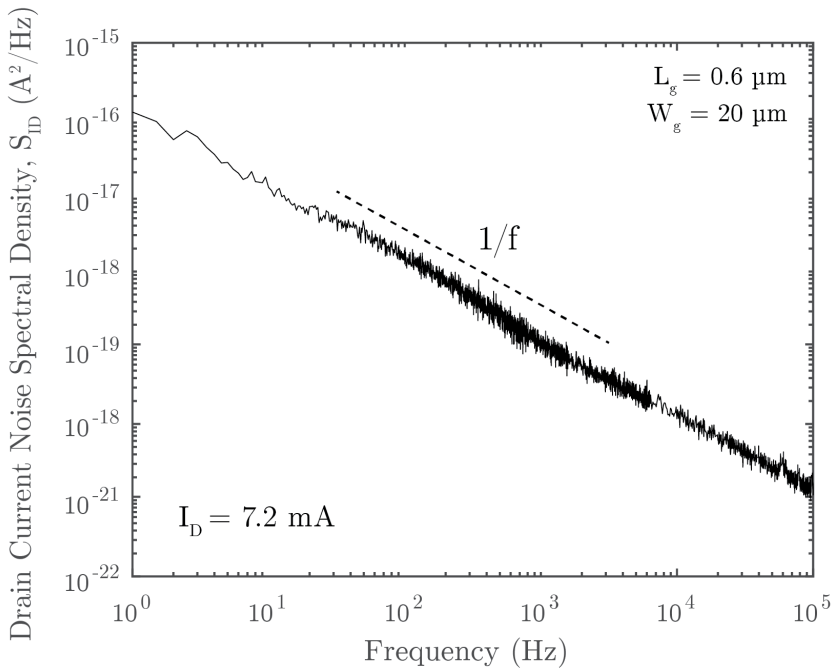

Figure 3.6: Typical drain current noise spectra illustrating 1/f noise.

Figure 3.7 depicts the typical configuration of an nMOS device.

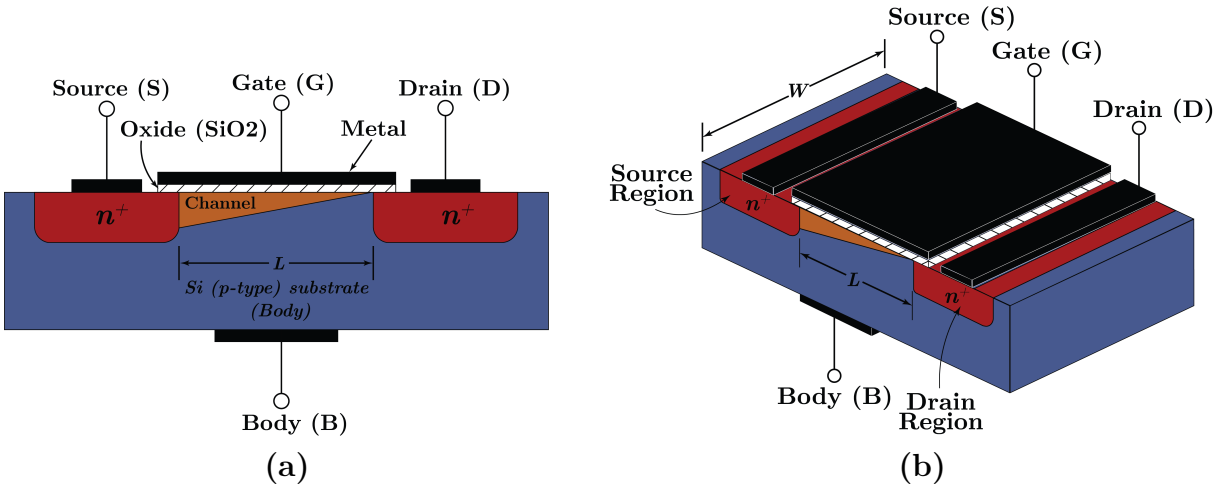

Figure 3.7: nMOS device fabrication configuration.

A typical Si MOSFET contains a high input resistance at the gate terminal. This is due to the oxide (SiO2) layer, which acts as an isolation layer as SiO2 has an extremely high resistance; $10^{14} - 10^{16}$ Ω-cm [29]. Hence, an nMOS device has no input current (disregarding leakage current, which does not flow through the SiO2 layer) and furthermore it is not possible to measure the input noise of a MOSFET device. For this reason, the concept of equivalent input noise voltage (S_{VG}) must be examined.

It is known for a MOSFET that the ratio of change in drain current (I_D) to the change in gate voltage (V_G) is given by the transconductance (g_m) of the device. Therefore, calculating the following will give S_{VG} (V^2/Hz)

$$S_{VG} = \frac{S_{ID}}{g_m^2} \tag{3.8}$$

The measured transconductance (g_m) of the DUT for the bias conditions of interest is depicted in Figure 3.8, while an example of S_{VG} is illustrated in Figure 3.9.

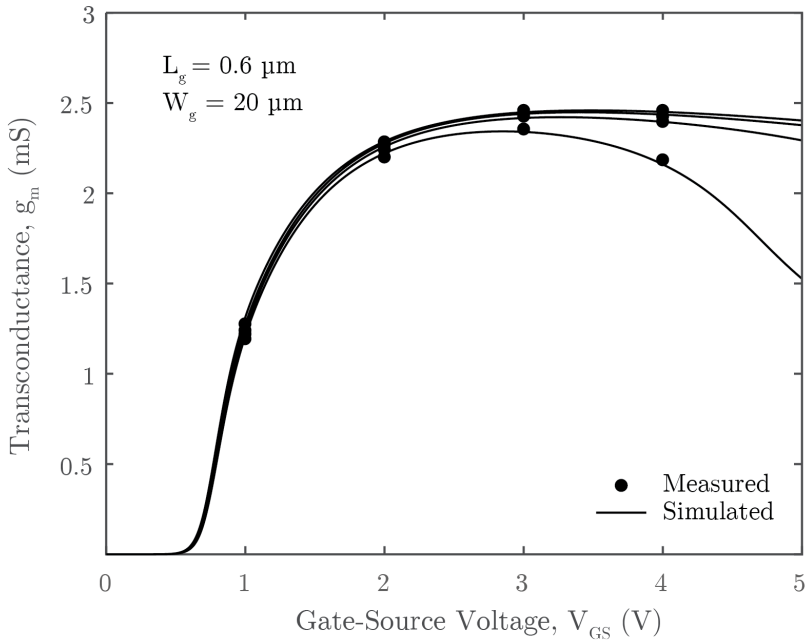

Figure 3.8: Measured vs simulated transconductance of industry supplied nMOS device.

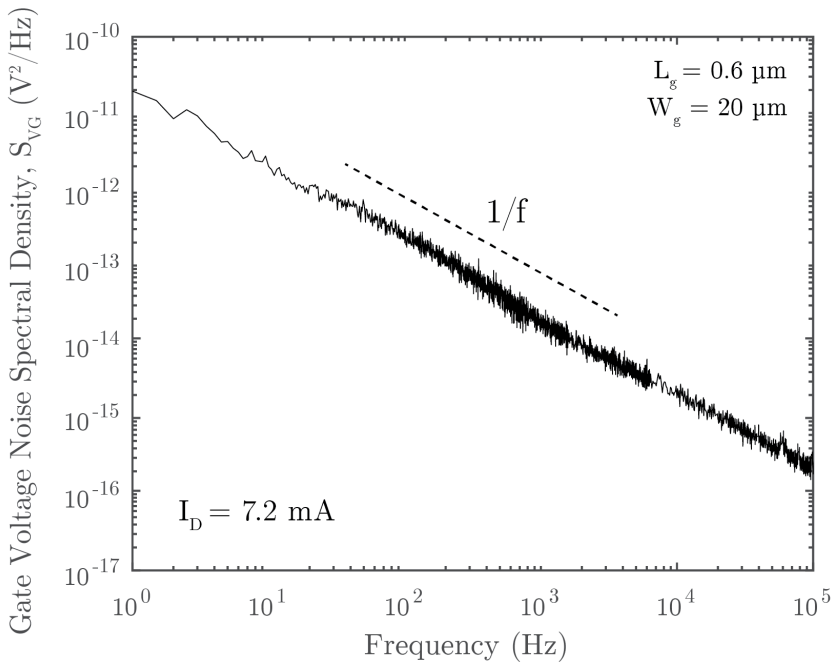

Figure 3.9: Equivalent input noise voltage noise spectra illustrating 1/f noise.

Chapter 4

Device modelling and data verification

4.1 Measurement system verification

In order to verify the resolution of the measurement system, the thermal noise of a resistor is measured. Preferably, a wire-wound or metal film resistor. The equation for calculating the thermal noise of a resistor was given in Equation (2.19). Hence, for a 100 kΩ resistor the thermal noise, in a 1 Hz bandwidth, is given as

$$\begin{aligned} S_v(f) &= 4KTR_D = 4 \times 1.38e^{-23} \times 298 \times 100e^{+3} \\ &= 1.645e^{-15}V^2/Hz \\ &\Rightarrow 40.558e^{-9}V/\sqrt{Hz} \end{aligned} \tag{4.1}$$

Figure 4.1 depicts the measured versus simulated/calculated thermal noise values of various resistor values. It is to be noted that the measured data in Figure 4.1 has been slightly modified in order to eliminate the intrinsic system noise that is typically present. This modification is the equivalent of passing the measured data through a digital low-pass filter which has a cutoff frequency of 1 Hz or lower.

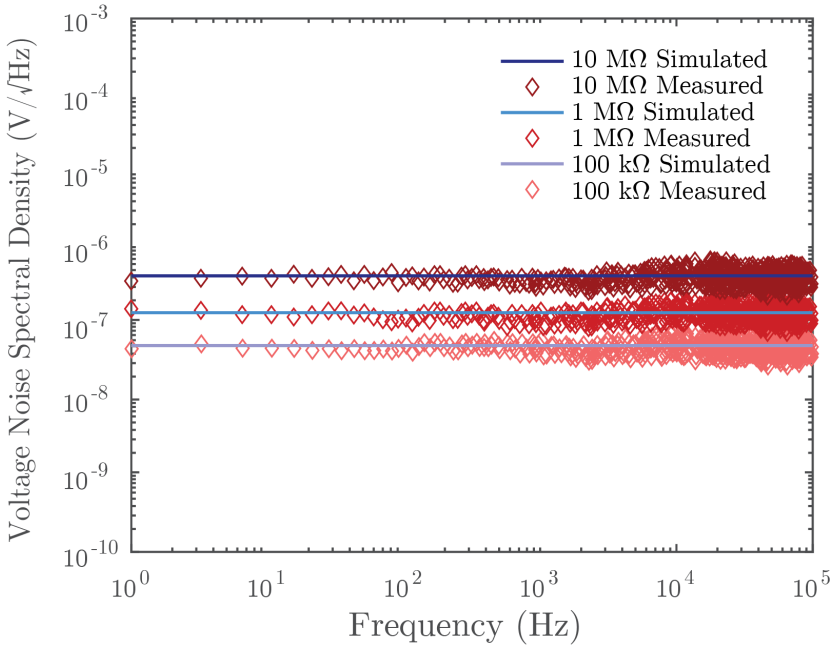

Figure 4.1: Measured vs. simulated noise for various resistances.

Once the system resolution has been verified, the DUT of interest can be incorporated into the measurement system and its DC conditions then verified. Verification of the DC bias currents is an important step as they form a reference when biasing the DUT for noise measurements. Furthermore, due to the configuration of the battery PSU, there exists a significant voltage drop across R_D such that it needs to be accounted for when applying bias to the DUT. It is advisable that the device terminal voltages are monitored whilst performing noise measurements, to ensure that the DUT is at the desired bias conditions.

In the case of this work, a DC model card was provided alongside the wafer devices by the industry partner. Therefore, a comparison can be made between the DC model card (simulation results) and the measured DC biasing conditions of the DUT. This is illustrated in Figure 4.2 and 4.3. A HP4145A SMU was used in order to obtain the DC performance of the DUT. Note that the difference between the measured and simulated data from $0 - 0.5$ V_{GS} in Figure 4.2 is due to the minimum current compliance limit of the HP4145A [30].

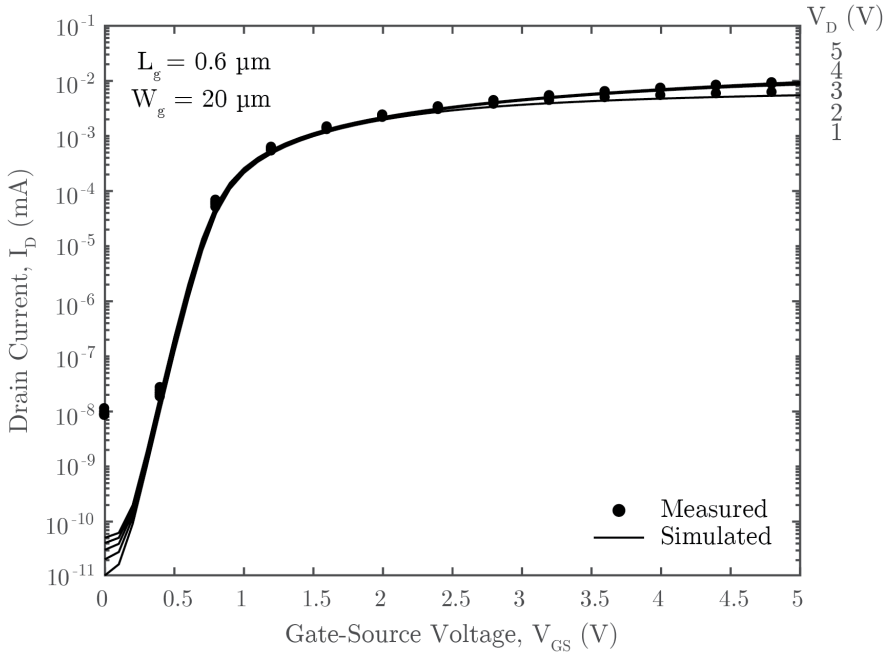

Figure 4.2: Measured and simulated drain current (I_D) vs. gate voltage (V_{GS}).

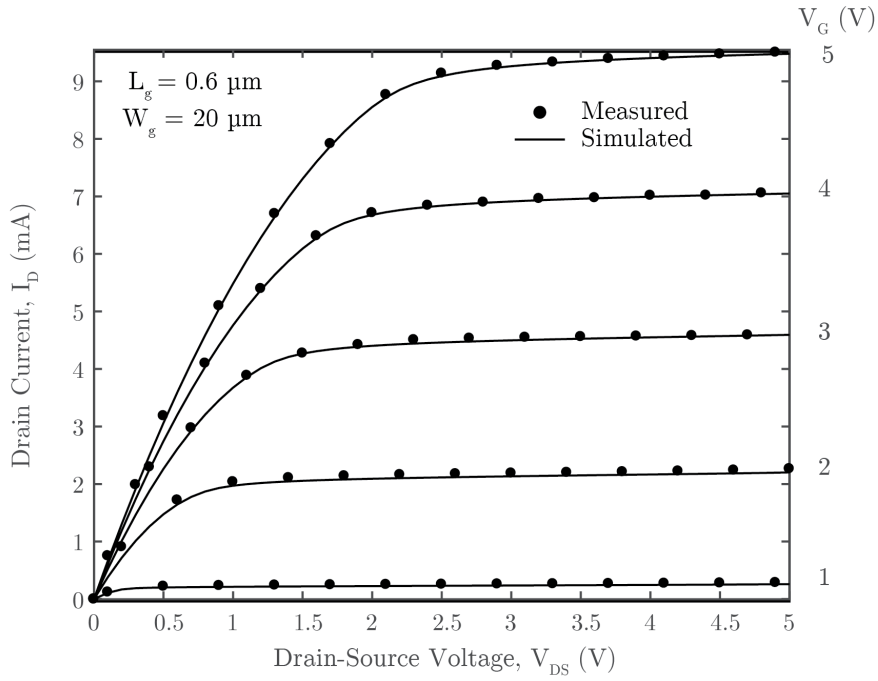

Figure 4.3: Measured and simulated drain current (I_D) vs. drain voltage (V_{DS}).

Figure 4.4 illustrates the recorded biasing conditions during the noise measurements compared to the measured DC only (I_D vs. V_{DS}, Figure 4.3) biasing conditions.

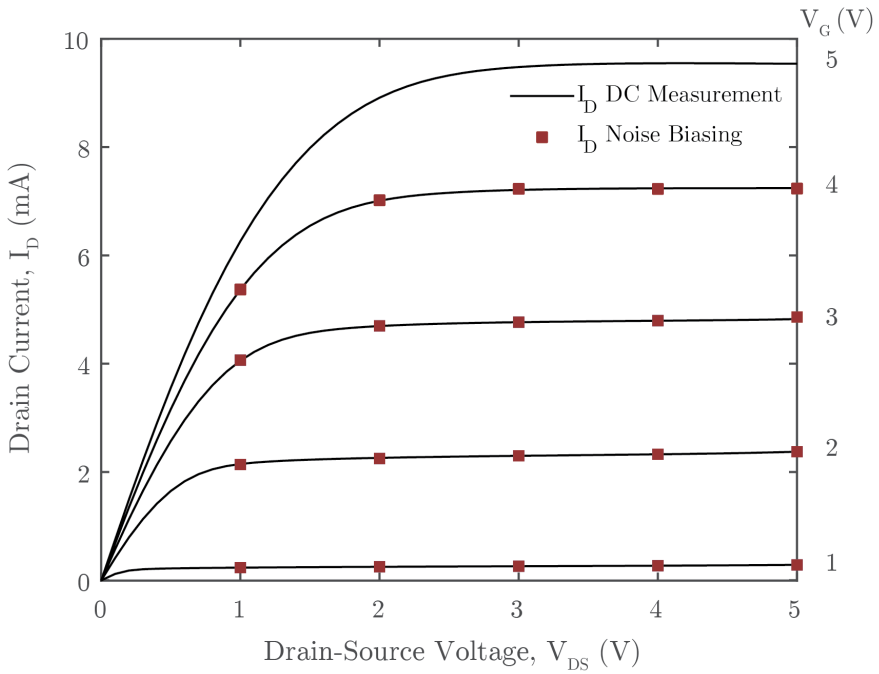

Figure 4.4: Biasing conditions recorded for DC only measurements compared to noise measurements.

If the data points do not overlay, as seen in Figure 4.4, it is necessary to ensure that the effects of device self heating are not present. Hence, in order to achieve reliable low-frequency noise measurements, it is important that the measurements are made at steady-state thermal conditions.

Only once the measurement setup has been verified should noise measurements be conducted. Figure 4.5 depicts the measured noise for variances of V_G while V_D is held constant. The measurements are repeated for different instances of V_D which pertain to the bias conditions of interest ($V_D = 1 - 5$V, not presented in this work). Figure 4.6 depicts the input referred voltage noise (S_{VG}) as calculated for the DUT. It can be seen that S_{VG} has a weaker dependence on V_G as opposed to V_D.

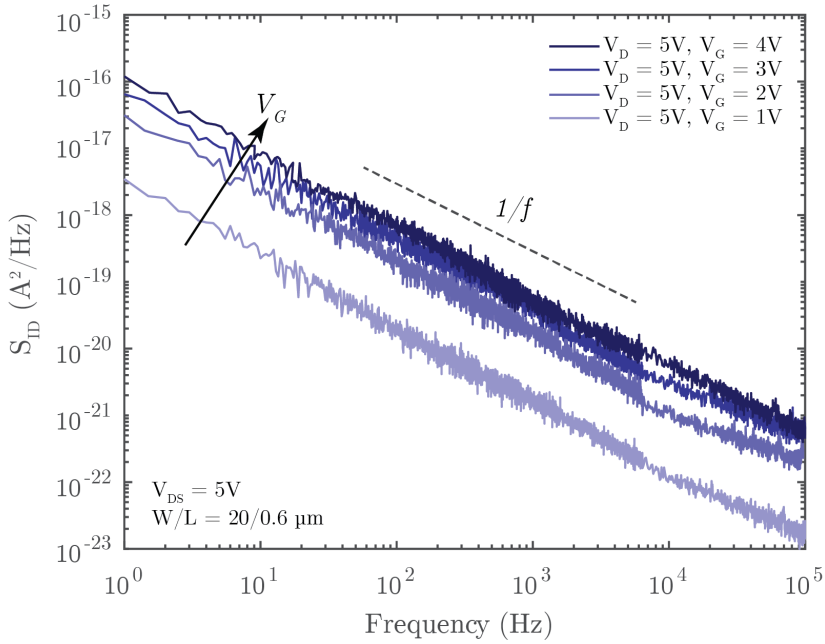

Figure 4.5: Measured on-wafer DUT noise for various gate voltages (V_G) while the drain voltage (V_D) is held constant.

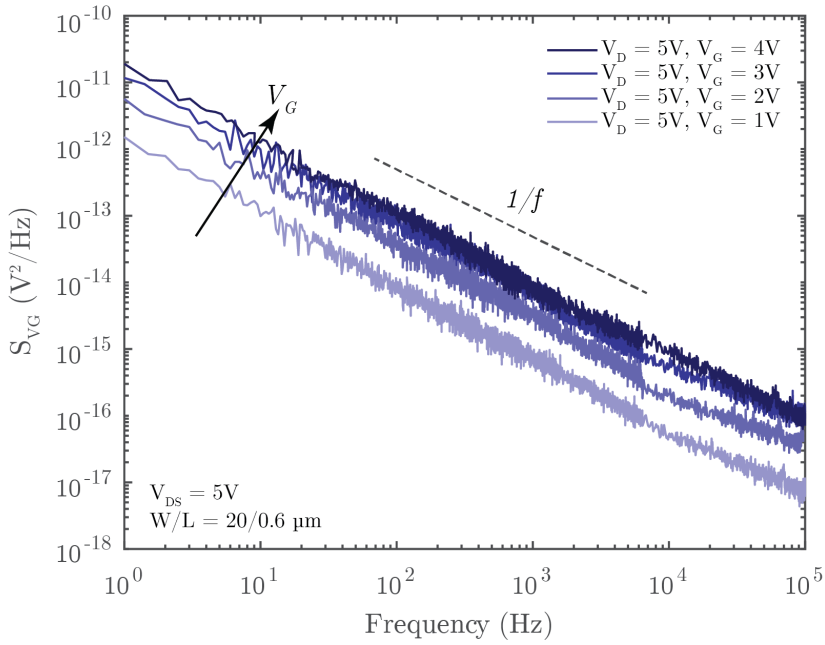

Figure 4.6: Input referred noise voltage of the on-wafer DUT for various gate voltages (V_G) while the drain voltage (V_D) is held constant.

4.2 Noise data quality verification by modelling

As can be seen from Figure 4.5 the measured noise pertains to the characteristics of $1/f$ noise. Therefore, by adopting a more systematic approach to the modelling stage can the obtained data be verified. This is done by means of the $1/f$ noise spectral density formula, which was given in Equation (2.28) as

$$S_{1/f} = \frac{KF \cdot I_D^{AF}}{f^{EF} C_{ox} L_{eff}^2}, \tag{4.2}$$

where KF is the $1/f$ noise coefficient, AF is the $1/f$ noise exponent, EF is the $1/f$ noise frequency exponent, I_D is the drain current (mA), f is the frequency (Hz), C_{ox} is the gate oxide capacitance per unit area and L_{eff} is the effective channel length (m). To put the $1/f$ noise parameters more simply, KF and AF both adjust the magnitude/scaling of the noise, with AF having less dependence (fine tuning) while KF has more dependence (coarse tuning) and EF is the slope of the noise, which in an ideal case is equal to unity.

If C_{ox} is not specified it may be calculated, given that T_{ox} is known, by the following

$$C_{ox} = \frac{\epsilon_{ox}}{T_{ox}}, \tag{4.3}$$

where T_{ox} is the oxide thickness and ϵ_0 is the permittivity of the Si02 oxide layer given by

$$\epsilon_{ox} = \epsilon_0 \times \epsilon_r, \tag{4.4}$$

where ϵ_0 is the permittivity of a vacuum ($8.85e^{-12}$ F/m), ϵ_r is the dielectric constant of the Si02 oxide layer (3.97) [29].

L_{eff} is given by

$$L_{eff} = L_{drawn} - 2\Delta L = L_{drawn} - 2 \cdot L_{int}, \tag{4.5}$$

where L_{drawn} is the mask level channel length. While for ΔL, the parameter L_{int} (length offset fitting parameter) represents the traditional manner from which ΔL is extracted.

If C_{ox} and L_{eff} are unknown, the more general formula may be used, given by

$$S_{1/f} = \frac{KF \cdot I_D^{AF}}{f^{EF}} \tag{4.6}$$

First, the data is to be plotted on a log-log scale where the slope (EF) can be extracted by applying a linear regression curve fitting, see Figure 4.7. The noise parameter EF is the negative of the slope. Thus, since the EF parameter is now known, Equation (4.2) can be reduced to the following

$$S_{1/f} \cdot f^{EF} = \frac{KF \cdot I_D^{AF}}{C_{ox} L_{eff}^2} = S_{1\,Hz} \tag{4.7}$$

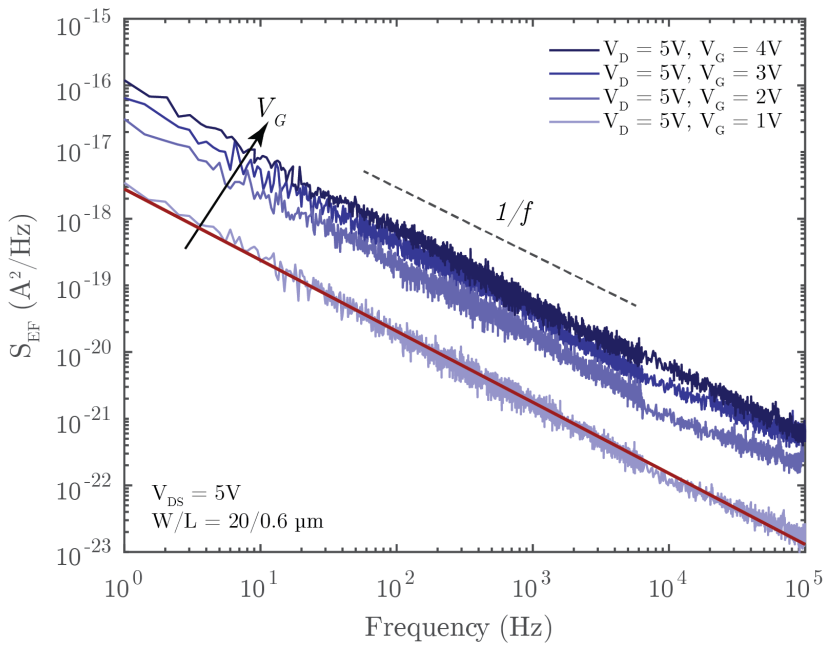

Figure 4.7: Log-log plot of data where the parameter EF can be extracted.

Second, the noise spectral density values at the frequency of 1 Hz ($S_{1\,Hz}$) can be extracted. These values are obtained in order to aid in the extraction of the remaining noise parameters; AF and KF. The extrapolated measurement results are obtained by multiplying the measured data by f^{EF}, as done so in Equation (4.7). This typically causes the measured data to have a flat response, as seen in Figure 4.8. The mean value of each

plot is taken, which corresponds to the value of $S_{1\,Hz}$. It is important to note that if the resulting plot does not have an entirely flat response then the mean value is to be taken across the range that has the least amount of variance (most flat).

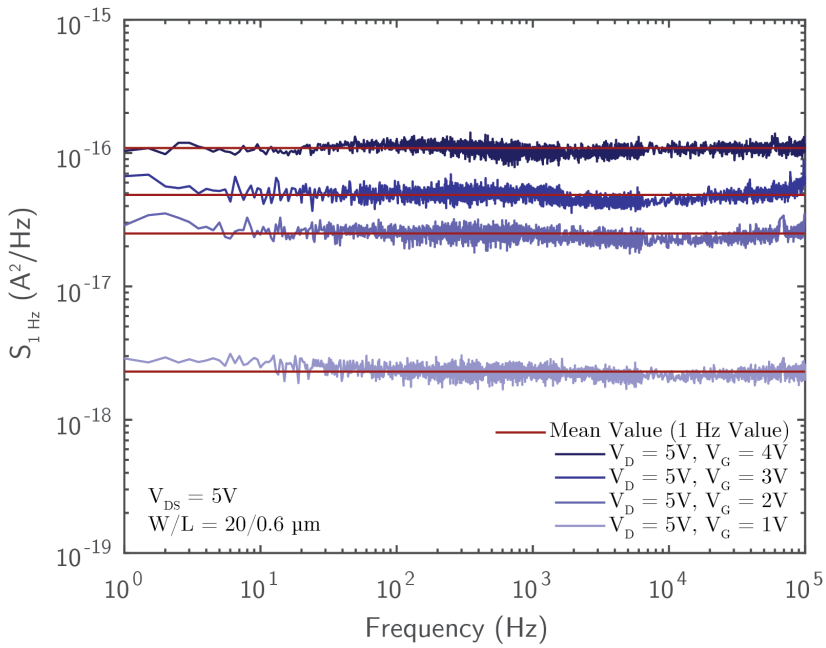

Figure 4.8: Log-log plot depicting the 1 Hz (mean) values of S_{ID} for varying values of V_G at a constant V_D.

Third, the 1 Hz (mean) values that have been obtained are then plotted on a log-log scale against their corresponding I_D noise bias current, as recorded from Figure 4.4. This is depicted in Figure 4.9.

Furthermore, by applying a logarithmic conversion to Equation (4.2) gives the following form

$$\log_{10}(S_{1\,Hz}) = AF \cdot \log_{10}(I_D) + \log_{10}\left(\frac{KF}{C_{ox}L_{eff}^2}\right) \tag{4.8}$$

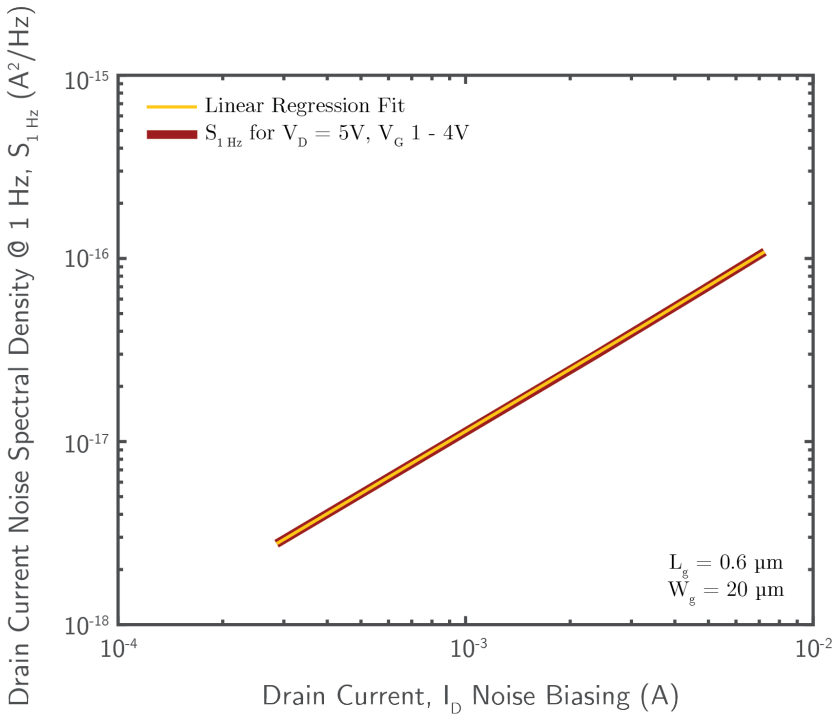

Figure 4.9: Log-log plot, prior to logarithmic conversion, depicting the 1 Hz (mean) values of S_{ID} for varying values of V_G at a constant V_D.

Thus, Equation (4.8) can be interpreted as a linear function of the form $y = mx + b$ where,

$$\begin{aligned} y &= \log_{10}(S_{1\,Hz}), \\ m &= AF, \\ b &= \log_{10}\left(\frac{KF}{C_{ox}L_{eff}^2}\right), \\ \Rightarrow KF &= C_{ox} \cdot L_{eff}^2 \cdot 10^b \end{aligned} \tag{4.9}$$

Figure 4.10 illustrates applying a linear regression fit once a logarithmic conversion has been performed with the linear function taking the form y = 1.106x - 13.5846.

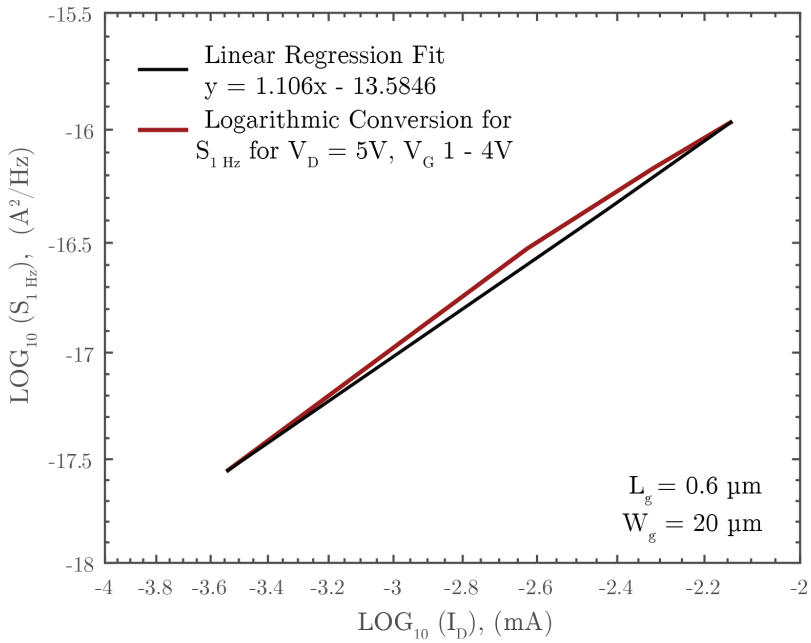

Figure 4.10: S_{1Hz} after applying a logarithmic conversion, depicting the 1 Hz (mean) values of S_{ID} for varying values of V_G at a constant V_D.

Thus, by applying the formulae from Equation (4.9) the $1/f$ noise parameters for the DUT can be obtained and are as follows

$$EF = \boxed{1.073}$$

$$AF = \boxed{1.106}$$

$$KF = 2.47e^{-3} \cdot (4.39e^{-7})^2 \cdot 10^{-13.5846}$$

$$\Rightarrow KF = \boxed{1.239e^{-29}}$$

4.3 Verification by simulation

With a complete set of extracted noise parameters, it is important to verify that these parameters comply with the measured data after the DUT model card has been updated with the extracted noise parameters. This is done by means of simulation in the electronic design automation (EDA) package LTSpice. A comparison between the measured data, simulated data and the model fitting is illustrated in Figure 4.11.

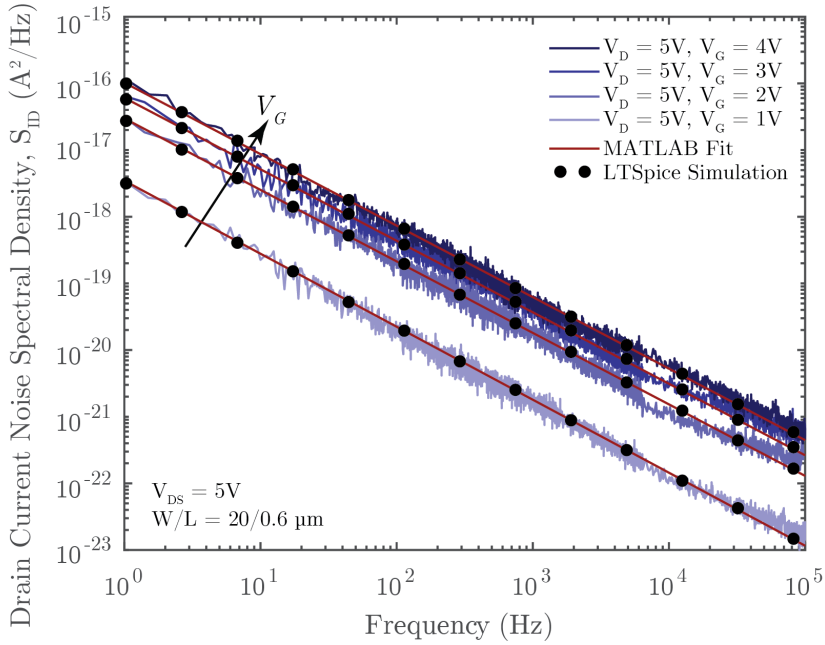

Figure 4.11: Measured S_{ID} vs. simulated S_{ID} with the calculated parameter extraction results overlaid.

It can be seen from Figure 4.11 that the simulated results give a very accurate prediction of the measured data.

Chapter 5

Conclusion and future work

In this work, a systematic and self-consistent framework for the characterisation, modelling and simulation of low-frequency noise which is present in Si MOSFETs has been presented. By accurately predicting such noise sources allows for complete optimisation in the performance of RF/wireless systems.

The work, in its entirety, has been shown to hold true for an on-wafer n-channel MOSFET. While there exists EDA packages which are capable of performing automatic noise parameter extraction, errors can arise due to improperly measured data thus leading to an inaccurate model. By adopting a manual approach, the measured data can be verified resulting in improvements in the accuracy of the noise model.

Due to the spatial limitations of this work, the framework that has been presented was completed for a drain voltage that is held constant. However, the bias conditions of interest in this work have been stated as $V_D = 1 - 5$V and $V_G = 1 - 4$V. Figure 5.1 and 5.2 depict the bias dependence of the drain current noise spectral density for the DUT.

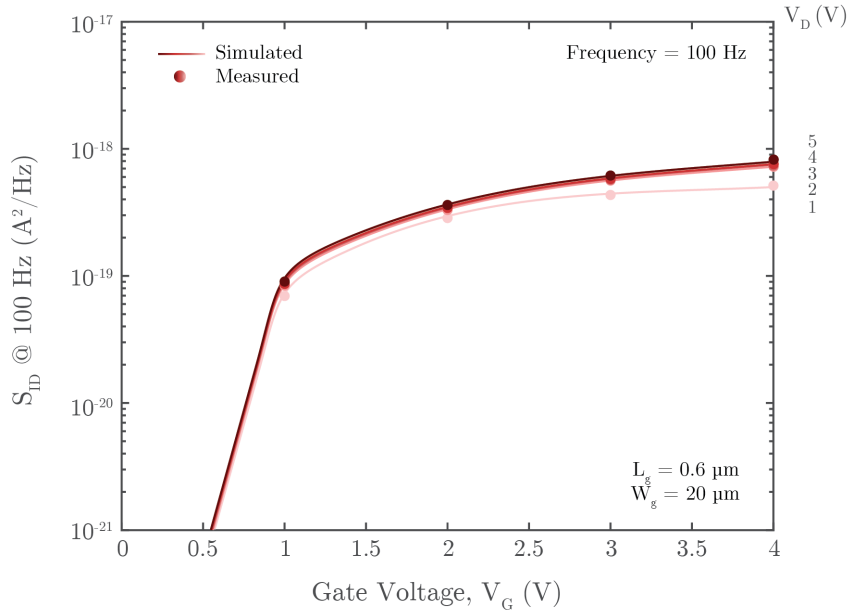

Figure 5.1: Bias dependence of drain current noise spectral density at 100 Hz for a drain voltage of 1 – 5V.

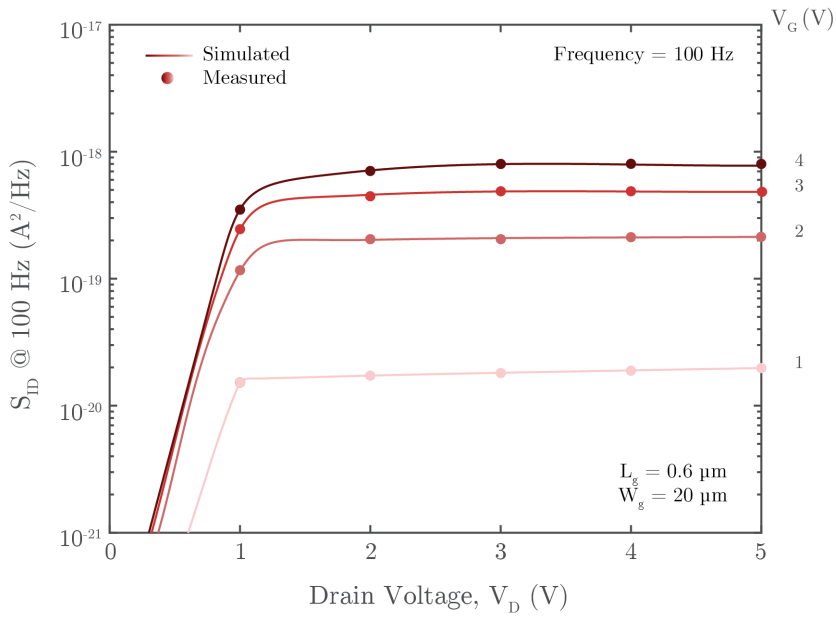

Figure 5.2: Bias dependence of drain current noise spectral density at 100 Hz for a drain voltage of 1 – 5V.

In order to obtain a more accurate noise model, it is vital that the noise parameter extraction process be done under all regions of MOSFET operation, notably in the subthreshold region which is absent from this work. Therefore, there exists the need to characterise the noise of the DUT in this work for all regions of operation, which can be done by following the framework that has been presented. This will allow for increased accuracy in the modelling of the intrinsic $1/f$ noise which is present in the DUT.

Appendix A

Noise measurements using the SR780 dynamic signal analyser

The following steps are necessary to enable communication between the PC and the SR780 Dynamic Signal Analyser:

A.1 GPIB

Depending on the manufacturer of the GPIB cable being used; Keysight or National Instruments (NI), the GPIB driver software (available from the manufacturer) must be installed on the host PC and configured to detect the GPIB controller connecting the SR780 to the USB port of the PC. Each of the two manufacturers have a software package available that helps the user to set up a communication link between the measurement equipment and the host PC; Keysight Connection Expert and NI Measurement & Automation Explorer (MAX). Within this software package the user can find all of the necessary information that is required for instrument control via GPIB.

A.2 MATLAB

While there exists a wide variety of software packages that enable instrument control, the use of MATLAB was deemed as the most suitable choice due to its simplicity. In order to use MATLAB for instrument control, MATLAB must be installed on the host PC, including the Instrument Control Toolbox. Once the software has been correctly installed, the MATLAB script in Appendix A.2.1 can be run in order to configure the SR780 dynamic signal analyser such that it is ready for noise measurements. Once the measurements have been completed, the script in Appendix A.2.2 can be run in order to 'dump' the data from the SR780 on to the host PC. Due to a bug within the SR780, the x-axis display of the SR780 must be in linear mode (not log) otherwise the equipment is unable to dump the data. The script in Appendix A.2.1 configures the SR780 to turn averaging off. This is done in order to allow the user to confirm all of the settings before the averaging begins. Once the settings have been verified, the averaging is set to 'ON' for the measurement averaging to begin. Only once the averaging is complete may the data be dumped on to the host PC (if averaging is being used).

A.2.1 MATLAB script to configure SR780

```
% Find a GPIB object.
sr780 = instrfind('Type', 'gpib', 'BoardIndex', 7, 'PrimaryAddress', 10, 'Tag', '');

% Create the GPIB object if it does not exist
% otherwise use the object that was found.
if isempty(sr780)
    sr780 = gpib('AGILENT', 7, 10); % BoardIndex (7) may be different for each PC. To confirm, run 'tmtool' and verify under 'Hardware -> GPIB'.
else
    fclose(sr780);
    sr780 = sr780(1)
end

% Required for 'DUMP'; 27200 = 800 lines, 13600 = 400 lines, 6800 = 200 lines, and 3400 = 100 lines. Please manually change ''sr780.InputBufferSize" on the next line to the corresponding FFT resolution of choice, else 'DUMP' command will not work.
sr780.InputBufferSize = 27200

% Connect to the SR780.
fopen(sr780);
```

```
% Verify that the SR780 object was successfully opened. Status ‘‘open" should be returned.
% get(sr780, 'Status')

% Initialise device
fprintf(sr780,'OUTX 0'); % Output to GPIB
fprintf(sr780,'MGRP 2,0'); % FFT Measurement
fprintf(sr780,'FAVG 2,0'); % Averaging off
% fprintf(sr780,'DFMT 0'); % Set single or dual display. Note: ‘DUMP' will give the data from both displays, if they're both active.

% Set frequency sweep
fprintf(sr780,'FBAS 2,1'); % Set base frequency to 102.4 kHz
fprintf(sr780,'FLIN 2,3'); % Set FFT resolution to 800 lines
fprintf(sr780,'FSPN 2,800'); % Set frequency span to 800 Hz

% Set window
fprintf(sr780,'FWIN 2,2'); % Hanning
fprintf(sr780,'PSDU 2,1'); % Turn on PSD units
fprintf(sr780,'XAXS 2,0'); % Set x-axis to linear scale. Note: Instrument can't seem to handle a data dump when x-axis is in log scale. Convert to loglog after data dump.

% Set measurement: FFT, View: Log Mag
```

```
fprintf(sr780,'MEAS 0,0'); % Display A: FFT1
fprintf(sr780,'MEAS 1,2'); % Display B: Time 1
fprintf(sr780,'UNIT 2,1'); % Display A and B: Set units to Vrms
fprintf(sr780,'VIEW 0,0'); % Display A: Log mag
fprintf(sr780,'VIEW 1,3'); % Display B: Real part

% Set input: AC, autograning off
fprintf(sr780,'I1CP 1'); % Channel 1 AC coupling
fprintf(sr780,'I1GD 1'); % Channel 1 grounding on
fprintf(sr780,'A1RG 0'); % Channel 1 autoranging off
fprintf(sr780,'IAOM 0'); % Auto offset off

% Set averaging
fprintf(sr780,'FAVM 2,1'); % RMS averaging
fprintf(sr780,'FAVN 2,100'); % Number of averages
fprintf(sr780,'FAVT 2,0'); % Average type: Linear

% Set output
fprintf(sr780,'PDST 3'); % Output port to the GPIB port.
fprintf(sr780,'PCIC 0'); % GPIB control to the host computer

% fclose(sr780);
```

A.2.2 MATLAB script for data dump from the SR780

```
% Find a GPIB object
sr780 = instrfind('Type', 'gpib', 'BoardIndex', 7, 'PrimaryAddress', 10, 'Tag', '');

% Create the GPIB object if it does not exist
% otherwise use the object that was found
if isempty(sr780)
    sr780 = gpib('AGILENT', 7, 10); % 'AGILENT' used for Agilent GPIB cable, if NI cable is used command becomes 'ni'
else
    fclose(sr780);
    sr780 = sr780(1)
end

% Required for 'DUMP' command; 27200 = 800 lines, 13600 = 400 lines, 6800 = 200
% lines, and 3400 = 100 lines
sr780.InputBufferSize = 27200

% Connect to the SR780.
fopen(sr780);

% Verify that the SR780 object was successfully opened. Status "open"
```

```
% should be returned.
get(sr780, 'Status')

%b1 = query(sr780,'DSPY ? 0\n') % Command to grab the Y-axis data only

b1 = query(sr780,'DUMP') % Command to grab both the X- and Y-axis data
b2=str2num(b1) % Convert the data to two columns
flushoutput(sr780) % Flush the SR780 output buffer

% Plot the two column 'DUMP' data, column one = frequency, column two = voltage
hold on
x=b2(:,1);
y=b2(:,2);
xlim ([-inf inf])
ylim ([-inf inf])
plot(x,y) % Divide y-axis by the gain of the SR560 times the gain of the device being measured
set(gca,'xscale','log');
set(gca,'yscale','log');

save('MeasurementX.txt','b2','-ascii') % Name the data file accordingly!
```

Appendix B

Battery-operated bias supplies

Custom-made battery-operated bias supplies were designed by Oya Sevimli [31]. The circuit diagrams are shown in Figure B.1.

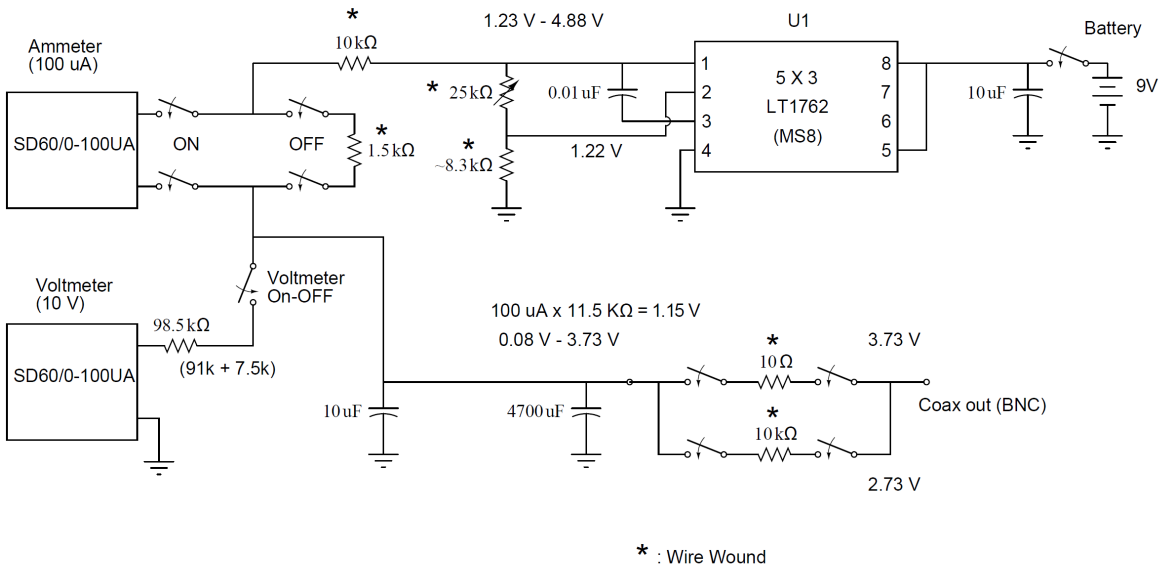

(a)

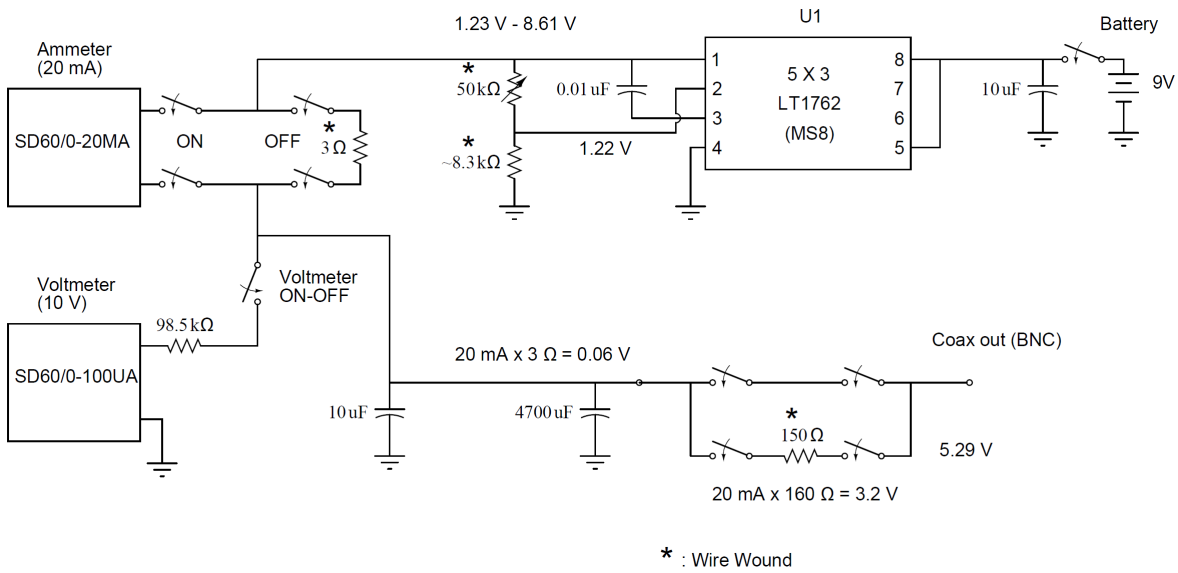

(b)

Figure B.1: Circuit diagrams of the custom-made battery-operated bias supplies: (a) gate supply, (b) drain supply.

Appendix C

Abbreviations

BNC	Bayonet Neill-Concelman
BPF	Band Pass Filter
CRT	Cathode Ray Tube
DC	Direct Current
DSA	Dynamic Signal Analyser
DUT	Device Under Test
EDA	Electronic Design Automation
EMI	Electromagnetic Interference
FFT	Fast Fourier Transform
LPF	Low-Pass Filter
MOSFET	Metal-Oxide-Semiconductor Field-Effect Transistor
nMOS	N-Channel MOSFET
PC	Personal Computer
PSD	Power Spectral Density
PSU	Power Supply Unit
RMS	Root-Mean-Square

RF	Radio Frequency
Si	Silicon
SiO2	Silicon Dioxide
SMU	Source Measure Unit
SPICE	Simulation Program with Integrated Circuit Emphasis
USB	Universal Serial Bus

Bibliography

[1] M. J. Deen and O. Marinov, "Noise in advanced electronic devices and circuits," in *Proc. Int. Conf. Noise and Fluctuations (ICNF)*, 2005, pp. 3-12.

[2] A. van der Ziel, *Noise in Solid State Devices and Circuits*, New York, John Wiley & Sons, Inc., 1986.

[3] F. Sischka, "Measuring and Modeling Electronic Device Noise," SisConsult, Magstadt, Germany. Apr. 27, 2015.

[4] R. Landauer, "The noise is the signal," *Nature*, vol. 392, pp. 658-659, 1998.

[5] M. Von Haartman, "Low-frequency noise characterization, evaluation and modeling of advanced Si- and SiGe-based CMOS transistors," PhD dissertation, Stockholm, 2006.

[6] W. Schottky, "Über spontane Stromschwankungen in verschiedenen elektrizitätsleitern," in *Annalen der Physik*, vol. 57, pp. 541-567, 1918.

[7] J. B. Johnson, "Thermal agitation of electricity in conductors," in *Physical Review*, vol. 32, pp. 97-109, 1928.

[8] H. Nyquist, "Thermal agitation of electric charge in conductors," in *Physical Review*, vol. 32, pp. 110-113, 1928.

[9] P. K. Nag. *Engineering Thermodynamics.* New Delhi: Tata McGraw-Hill Publishing Company Limited, 2008, pp. 119-121.

[10] "Thermal Johnson Noise Generated by a Resistor." Internet: http://123.physics.ucdavis.edu/week_2_files/Johnson_noise_intro.pdf [Aug. 21, 2017].

[11] J. C. Nallatamby, M. Prigent, M. Camiade, A. Sion, C. Gourdon, and J. Obregon. An advanced low-frequency noise model of GaInP-GaAs HBT for accurate prediction of phase noise in oscillators. *IEEE Transactions on Microwave Theory and Techniques,* 53(5):1601-1612, May 2005.

[12] J. B. Johnson, *Phys. Rev.*, **26**, 71 (1925) vol. 32, pp. 97-109, 1928.

[13] W. Johnson, *Phys. Rev.*, **28**, 74 (1926) vol. 32, pp. 97-109, 1928.

[14] M. Surdin, "Fluctuations in the thermionic current and the 'flicker effect'," *J. Phys. Radium*, vol. 10, pp. 188-189, 1939.

[15] A. L. McWorther, "1/f noise and related surface effects in germanium," Massachusetts Institute of Technology Lincoln Laboratory Report 80, May 1955.

[16] A. L. McWorther, "1/f noise and germanium surface properties," in *Semiconductor Surface Physics*, pp. 207-228, Philadelphia: University of Pennsylvania Press, 1957.

[17] F. N. Hooge, "$1/f$ noise," *Physica*, vol. 83B, pp. 14-23, 1976.

[18] F. N. Hooge and L. K. Vandamme, "Lattice scattering causes 1/f noise," *Physics Letters*, vol. 66A, pp. 315-316, 1978.

[19] S. Machlup, "Noise in semiconductors: spectrum of a two-parameter random signal," *J. Appl. Phys.*, vol. 25, pp. 341-343, 1954.

[20] F. N. Hooge, "1/f noise is no surface effect," *Phys. Lett. A*, vol. 29a, pp. 139-140, 1969.

[21] F. N. Hooge, "Discussion of recent experiments on 1/f noise," *Physica*, vol. 60, pp. 130-144, 1972.

[22] R. A. Wilcox, J. Chang, and C. R. Viswanathan, "Low-temperature characterization of buried-channel NMOST," *IEEE Trans. Electron Devices*, vol. 36, pp. 1440-1447, 1994.

[23] K. K. Hung, P. K. Ko, C. Hu and Y. C. Cheng, "A unified model for the flicker noise in metal-oxide-semiconductor field-effect transistors," in *IEEE Transactions on Electron Devices*, vol. 37, no. 3, pp. 654-665, Mar 1990.

[24] A. Arnaud and A. Hoffmann, "A complete compact model for flicker noise in MOS transistors," *2015 IEEE 6th Latin American Symposium on Circuits & Systems (LASCAS)*, Montevideo, 2015, pp 1-4.

[25] Model SR780 Network Signal Analyser User's Manual Rev. 2.4. (Stanford Research Systems, Inc., 2005).

[26] Model SR560 Low-Noise Preamplifier User's Manual Rev. 3. (Stanford Research Systems, Inc., 2013).

[27] V. Gabriel, 'Electronic Noise and Interfering Signals: Principles and Applications. -Springer- Verlag Berlin Heidelberg, 2005. 709 p.

[28] F. Walls, D. Percival, and W. Irelan, "Biases and variances of several FFT spectral estimators as a function of noise type and number of samples." In *Proceedings of the 43rd Annual Symposium on Frequency Control*, pp. 336-341, May-Jun 1989.

[29] "General Properties of Si, Ge, SiGe, SiO2 and Si3N4," Virginia Semiconductor, Fredericksburg, VA, Mar. 10 2012.

[30] Model 4145A Semiconductor Parameter Analyzer Operation and Service Manual. (Hewlett-Packard, LTD., 1982).

[31] O. Sevimli, 'Measurement and modelling of low-frequency noise in gallium-arsenide base heterojunction bipolar transistors for phase-noise simulation', Macquarie University, 2012.